$IN-02$

1626

$P.84$

Transonic Aerodynamics of Dense Gases

Sybil Huang Morren
Lewis Research Center
Cleveland, Ohio

NASA

Transonic Aerodynamics of Dense Gases

Sybil Huang Morren
National Aeronautics and Space Administration
Lewis Research Center
Cleveland, Ohio 44135

Abstract

Transonic flow of dense gases for two-dimensional, steady state, flow over a NACA 0012 airfoil was predicted analytically. The computer code used to model the dense gas behavior was a modified version of Jameson's FLO52 airfoil code. The modifications to the code enabled modeling the dense gas behavior near the saturated vapor curve and critical pressure region where the fundamental derivative, Γ, is negative. This negative Γ region is of interest because the nonclassical gas behavior such as formation and propagation of expansion shocks, and the disintegration of inadmissible compression shocks may exist. The results of this study indicated that dense gases with undisturbed thermodynamic states in the negative Γ region show a significant reduction in the extent of the transonic regime as compared to that predicted by the perfect gas theory. The results of the thesis support existing theories and predictions of the nonclassical, dense gas behavior from previous investigations.

Acknowledgements

I thank my advisors, Dr. Mark Cramer and Dr. Saad Ragab, for their guidance, patience, and endurance during the course of this work. Dr. Cramer's enthusiasm and in-depth knowledge has given me a deeper understanding and appreciation in the areas of thermodynamics and gasdynamics. Also, he has sparked a great interest in me to pursue future studies of BZT fluids. Dr. Ragab's expertise in fluid dynamics, numerical methods and his familiarity with computational fluid dynamic codes contributed heavily to the completion of this research work. I also thank my committee members, Professor C.W. Smith and Dr. Carl Prather, for their time and effort in this endeavor.

Table of Contents

Chapter 1

Introduction

The purpose of this thesis is to investigate an airfoil flow environment for dense gases which exhibit nonclassical gasdynamic characteristics such as the formation and propagation of expansion shocks. The behavior of such fluids are referred to as nonclassical gasdynamics because their fluid characteristics are often contrary to those predicted by perfect gas theory. The nonclassical fluids are of interest because their behavior can not be predicted by the perfect gas theory. The potential benefits for these fluids maybe realized when these fluids are employed as the turbomachinery working fluid. Increased efficiency of the turbomachinery, extended life cycle of turbines, reduced hardware design requirements, and increased hardware reliability are only a few of the advantages which may be possible with the nonclassical gasdynamic working fluid.

The analytical predictions for the nonclassical gasdynamic fluids, hereafter referred to as the Bethe[1]-Zel'dovich[2,3]-Thompson[4] (BZT) fluids, were generated with FLO52. FLO52 is a two dimensional, steady state, Euler solver airfoil code developed by Dr. Anthony Jameson of Princeton University. The modifications to FLO52 involved removing all expressions which contain perfect gas thermodynamic assumptions. The perfect gas expressions were replaced with the corresponding expressions for the modeling the BZT fluids.

1

The BZT fluids offer numerous advantages for turbomachinery applications because they have the potential of supporting subsonic flow for high freestream Mach number conditions and/or high blade angles of attack. That is, for unusually high freestream flow speeds and high blade angles of attack, no compression shocks will be encountered. Energy losses due to compression shocks would be eliminated. Adverse pressure gradient effects resulting from compression shocks would not exist. As a result, losses from shock-induced boundary layer flow separation would also be eliminated.

The BZT fluids contain finite regions where the fluid fundamental derivative[4],

$$\Gamma = \frac{1}{\rho}\frac{\partial(\rho a)}{\partial \rho}\bigg|_{s}$$

(1.0)

is negative. Here, a, ρ, and s, are the thermodynamic sound speed, density, and entropy, respectively. The fundamental derivative characterizes the nonlinearity of a fluid. A fluid which remains solely in a thermodynamic region of negative Γ will admit expansion shocks only. Details of the shock existence theory are presented later. Fluids with high specific heats are most likely to exhibit BZT fluid characteristics[1,2,5].

An alternate form of the fundamental derivative is given by

$$\Gamma = \frac{v^4}{2a}\left(\frac{\partial^2 P}{\partial v^2}\right)_s$$

(1.1)

where v is the specific volume. Inspection of Equation (1.1) indicates that the fundamental derivative is proportional to the curvature of an isentrope in the P - v plane and

2

has the same sign as $\left.\dfrac{\partial^2 P}{\partial v^2}\right|_s$.

Fluids with solely positive fundamental derivative values can be shown to admit only compression shocks. An example of a strictly positive Γ fluid is the perfect gas. Consequently, the perfect gas admits only compression shocks. Expansion shocks in perfect gases disintegrate into expansion fans. The classical gasdynamic phenomena, such as sonic conditions obtained at minimum cross sectional area (i.e., a nozzle throat) for internal flow, Fanno line flow, and shock conditions for airfoils have been analyzed for the perfect gas model.

Little interest in the BZT fluids was evident until the 1970's and 1980's. The only significant works prior to this time were conducted by Bethe[1] and Zel'dovich[2,3]. In 1942 Bethe[1] determined that the region of negative nonlinearity existed near the saturated vapor line in the vicinity of the critical pressure. Bethe considered many fluids which could exhibit negative nonlinearity, but he argued that the practical applications of these fluids would still be in the positive Γ region. Bethe and Zel'dovich[2] speculated that the van der Waals equation of state would simulate the gas behavior of the fluids which exhibit negative Γ values. They also determined that a fluid which could exhibit negative nonlinearity would necessarily possess large specific heats, i.e., $C_v/R \gg 10$.

In the early 1970's Thompson and Lambrakis[4,5,6] published their work on negative Γ fluids. It was Thompson[4] who did the first work for BZT fluids in steady state isentropic flow, Fanno line flow, and weak shock theory. In 1972 Lambrakis and Thompson[5] provided evidence that many real fluids contained finite regions of negative nonlinearity near the saturated vapor curve near critical pressure, as predicted earlier by Bethe[1] and

3

Zel'dovich[2,3]. Thompson and Lambrakis[6] also investigated fluid behavior of gases which exhibited both positive and negative nonlinearities.

In the mid 1980's much work in the area of BZT fluids which contain both positive and negative nonlinearities was conducted by Cramer and Kluwick[7], Cramer et. al. [8], Cramer and Sen[9,10], and Cramer[11,12,13]. The behavior of fluids with both positive and negative Γ values differ from those which have strictly positive or strictly negative values of the fundamental derivative.

This study concentrates on describing BZT fluid flow environments for a NACA 0012 airfoil. In the following sections, discussions of the BZT fluid shock existence theory, analytical analysis employing the van der Waals equation of state, and BZT fluid results are presented. The results support the BZT fluid theories and show a tremendous reduction in the extent of the transonic regime as compared to the extent predicted by the perfect gas theory.

Chapter 2

General Theory

The gasdynamic theory for the BZT fluids is based upon relations which hold true for general fluids. This section begins with the classical gasdynamic analysis and expand to the shock existence theory which is specific to BZT fluids. The BZT fluid analysis for external flow over an airfoil is based upon conventional, single-phase, Navier-Stokes fluids. The flow is assumed to be compressible, inviscid, and two dimensional; therefore, the Navier-Stokes equations simplify to the Equations of (2.0).

$$\frac{\partial \rho}{\partial t} + \frac{\partial(\rho U)}{\partial x} + \frac{\partial(\rho V)}{\partial y} = 0 \qquad (2.0a)$$

$$\frac{\partial(\rho U)}{\partial t} + \frac{\partial\left(\rho U^2 + P\right)}{\partial x} + \frac{\partial(\rho UV)}{\partial y} = 0 \qquad (2.0b)$$

$$\frac{\partial(\rho V)}{\partial t} + \frac{\partial\left(\rho V^2 + P\right)}{\partial x} + \frac{\partial(\rho VU)}{\partial y} = 0 \qquad (2.0c)$$

$$\frac{\partial(\rho E)}{\partial t} + \frac{\partial(\rho UH)}{\partial x} + \frac{\partial(\rho VH)}{\partial y} = 0 \qquad (2.0d)$$

Often referred to as the Euler equations, Equations (2.0a) through (2.0d) represent the continuity, momentum in the x direction, momentum in the y direction, and the energy equation, respectively. The two additional equations required to form a closed system of

equations are the equations of state, and the internal energy equation.

The first term in each equation from Equations (2.0) represents the local rate of change of the conserved element. The second and third terms of the Equations (2.0) are the corresponding fluxes and pressure forces. The quantities of U and V are the velocity components in the x and y directions. The pressure, density, total internal energy, and total enthalpy are shown as P, ρ, E, and H. Equations (2.0) are the governing differential equations used in the BZT fluid analysis.

General aerodynamic analysis classifies fluid flow into compressible and incompressible flow. The density of an incompressible flow is for all practical purposes considered to be constant; while for compressible flow, the density may vary greatly. The science of thermodynamics describes the physics of energy relations or transformations and is incorporated in the analysis for both incompressible and compressible flow. However, the thermodynamic effects are extensive in compressible flow due to changes in kinetic energy, internal energy, density, and gas temperature which are characteristic of compressible gases. The analysis of compressible flow is more specifically referred to as gasdynamics. An important index used for describing the gas velocity is the Mach number which is defined as the ratio of the flow velocity to the thermodynamic sound speed. Fluid velocities equal to the speed of sound are referred to as sonic flows. Fluid velocities greater than the speed of sound are referred to as supersonic, while those below the speed of sound are termed subsonic.

In conventional gasdynamics, flows which have reached sonic velocities or greater may result in shock waves. The shock waves may be of two types, namely compression or expansion shocks. Compression shocks decelerate supersonic flow across the shock.

6

Pressure, density, entropy, and temperature increase across a compression shock. Unfavorable gas behavior results, such as shock-induced boundary layer separation, and enthalpy and pressure losses. In a rarefaction or expansion shock, the flow is accelerated through a shock; and the pressure, density, and enthalpy decrease across an expansion shock. The supersonic to subsonic transition may also occur across expansion shocks just as it does for compression shocks. In both shock conditions the entropy across the shock increases; and both types of shocks result in an irreversible thermodynamic process. Since expansion shocks provide a favorable pressure gradient for boundary layer separation, it appears that a major loss mechanism can be eliminated or minimized through the use of fluids admitting only expansion shocks.

Admissible shock conditions for general fluids are determined by

$$\rho_1 V_1 = \rho_2 V_2 = \dot{m} \tag{2.1a}$$

$$P_1 + \dot{m} V_1 = P_2 + \dot{m} V_2 \tag{2.1b}$$

$$e_1 + \frac{P_1}{\rho_1} + \frac{V_1}{2} = e_2 + \frac{P_2}{\rho_2} + \frac{V_1}{2} \tag{2.1c}$$

$$\dot{m}(s_2 - s_1) \geq 0 \cdot \tag{2.1d}$$

The Equations (2.1) are the continuity, momentum, energy, and entropy inequality, respectively, for a stationary, normal shock. They may be applied to a moving shock by transformation to an appropriate frame of reference. The solution to this system of equations represents all possible upstream and downstream conditions which may be reached through the dynamic process of a shock. Equations (2.1) are known as the

7

Rankine-Hugoniot shock jump conditions and are found in the gasdynamic literature (e.g. John[14], Anderson[15], or Bertin[16]).

These conditions may be rewritten as

$$[\rho V] = 0 \qquad (2.2a)$$

$$V_1 V_2 = \frac{[P]}{[\rho]} \qquad (2.2b)$$

$$[h] = \frac{1}{2}[P]\frac{\rho_1 + \rho_2}{\rho_2 \rho_1} \qquad (2.2.c)$$

$$[s] \geq 0 \qquad (2.2d)$$

where $[X] = X_2 - X_1$. The first equation is simply the continuity equation. The second is the result of the combination of the mass and momentum equations. The third equation is known as the Hugoniot equation, and is obtained by combining the continuity, momentum, and energy equation. The Hugoniot equation contains purely thermodynamic parameters; therefore, all solutions to equation (2.2c) correspond to thermodynamic states which may be connected by a shock wave. Figure 2.0 is a sketch of the Hugoniot equation for a BZT fluid. This curve is often referred to as the shock adiabat.

Now consider the shock existence conditions for general fluids. A given shock condition will be admissible only if the Rayleigh line connecting the proposed upstream and downstream states lies entirely above or below the shock adiabat. The Rayleigh line is defined as a straight line connecting any two points in a $P - v$ diagram where the end points denote the upstream and downstream states. If the Rayleigh line lies above the

8

shock adiabat, a compression shock ($P_2 > P_1$) is the admissible shock condition. Figure 2.0 depicts compression shock conditions for curves with state points 1 to 2, and 3 to 4. If the Rayleigh line lies below the shock adiabat, an expansion shock ($P_2 < P_1$) is admissible for the proposed shock condition. One example of an expansion shock is represented by the Rayleigh line between state points 2 and 3. Therefore fluids with positive shock adiabat curvatures admit compression shocks; and those with negative curvature shock adiabats admit expansion shocks. Admissible shocks will remain in the flow as discontinuities. Inadmissible shocks will undergo either a partial or total disintegration.

Previously the admissible shocks were shown to be related to the curvature of the shock adiabat. Now the relationship of the fundamental derivative to admissible shocks will be discussed. The fundamental derivative given in Equation (1.1) may be shown to be proportional to the curvature of the isentrope[13]. The sign of the fundamental derivative may also be shown to determine the direction of curvature of the shock adiabats as well. In general it can be shown that the slopes and the curvatures of the shock adiabat are identical to those of the isentropes at the same point, i.e.,

$$\lim_{v_2 \to v_1} \frac{d^2 P_2}{dv_2^2} = \left(\frac{\partial^2 P}{\partial v^2}\right)_S (P_1, v_1) \qquad (2.3)$$

Details of the derivation of equation (2.3) may be found in Reference 13.

Thus, fluids for which the fundamental derivative is positive everywhere also have positive shock adiabat curvatures which indicate compression shocks are the only admissible shock type. The perfect gas is an example of such a fluid; and therefore, admits only compression shocks. For fluids with strictly negative fundamental derivative values, the

shock adiabat curvature is also negative and indicates admissible expansion shocks. For fluids which contain mixed nonlinearity ($\Gamma > 0$ and $\Gamma < 0$), the shock adiabat will contain inflection points. The fluid of Figure 2.0 is such a fluid with both positive and negative values of Γ. Both types of shocks, possibly from the same upstream state, may occur when mixed nonlinearity is present.

Most classical gasdynamic theory involves the assumption of perfect gas behavior. The perfect gas equation of state,

$$P = \rho RT \qquad (2.4)$$

where P is the pressure, ρ is the density, R is the gas constant, and T is temperature, leads to convenient simplifications of gasdynamic relations. One of the motivations for the use of the perfect gas model is its simplicity and accuracy when applied to many real gases at atmospheric conditions. A real fluid's compliance to perfect gas behavior may be quantified by a parameter called the compressibility factor

$$Z = \frac{Pv}{RT} \qquad (2.5)$$

where Z is the compressibility factor, and v is the fluid specific volume.

According to Equations (2.4) and (2.5), a perfect gas has a compressibility factor of unity. A skeleton sketch of the compressibility chart for nitrogen is given in Figure 2.1. Any thermodynamic conditions which result in a compressibility factor other than unity are deviations from ideal gas behavior. In general, the perfect gas model is based upon the assumption of widely spaced molecules and negligible molecular interaction. Therefore the perfect gas equation clearly is not valid as a fluid approaches the saturated vapor curve

10

where molecular interaction is significant.   More detailed discussions of the perfect gas regime may be found in Van Wylen and Sonntag[17].

The perfect gas model is not adequate for analytical simulation of the negative Γ fluids. The thermodynamic region of interest for observing nonclassical gasdynamic characteristics (i.e. the region of negative Γ) has been determined by Bethe and Zel'dovich to be located near the saturated vapor curve and near critical pressures as shown in Figure 2.2. For reasons previously stated, the perfect gas model is invalid in the dense gas regime; and therefore, cannot accurately simulate the negative Γ region.

To successfully simulate fluid behavior in the dense gas region, a more comprehensive equation of state must be employed. The van der Waals equation

$$P = \frac{RT}{v-b} - \frac{\alpha}{v^2}$$

$$(2.6)$$

or
$$P = \frac{\rho RT}{1-b\rho} - \alpha\rho^2$$

is known as a generalized equation of state, which means that it holds for generalized (i.e., real gas) behavior, and should model fluids in dense gas region sufficiently.   The coefficients α and b are corrections for the intermolecular forces of attraction and repulsion between the molecules, and for the volume occupied by the molecules. These van der Waals coefficients can be evaluated from the critical point data.

For the generalized gas the critical isotherm at the thermodynamic critical point has a slope and curvature of zero. Therefore the first and second derivatives of the isotherm are zero at the critical point. The van der Waals coefficients are evaluated at this inflection point and

11

are

$$v_c = 3b$$

$$\alpha = \frac{27}{64}\frac{R^2 T_c^2}{P_c} \qquad (2.7)$$

$$b = \frac{RT_c}{8P_c}$$

where the critical point values of temperature, pressure, and specific volume are shown respectively as T_c, P_c, and v_c. The critical compressibility factor for a van der Waals fluid is $Z_c = 0.375$. This critical compressibility value was used throughout this thesis.

The van der Waals equation of state was employed successfully by Bethe[1], Zel'dovich[2], Thompson and Lambrakis[6], Cramer and Sen[9,10], Cramer[11,13], and others for modelling fluids with regions of negative Γ. More exact equations such as the Martin-Hou equation of state have been used. Examples of Martin-Hou equation calculations may be found in Table 2.0[18] and in Figure 2.3[5]. The Martin-Hou equation is regarded as one of the most realistic equation of state for power systems. However, the more complicated equations of state do not improve upon the qualitative results of the van der Waals model. Therefore, the van der Waals equation of state was deemed reasonable and sufficient for the present purpose.

Chapter 3

Analytical Approach

In order to analytically simulate the flow characteristics of BZT fluid flows, the FLO52 airfoil code by Anthony Jameson of Princeton University was modified by removing all influences of the perfect gas assumption and replacing them with the corresponding van der Waals gas equations. FLO52 is a two dimensional, steady state, finite volume airfoil code. Such finite volume codes have been extensively tested, and are well understood for perfect gases; therefore FLO52 was selected as the tool for the BZT analysis in this study. Although FLO52 has the multi-grid generation capability, the single grid generation option was used when modeling the BZT fluids.

The numerical solution scheme for FLO52 is based upon an explicit, semidiscrete finite volume scheme with implicit residual smoothing. The implicit nature of the solution allows the use of large time steps. The semidiscretizaton method is similar to finite differencing methods in that the difference representation is used to approximate the differential terms in the equations. However in the finite volume method the dependent variables are assumed to be known at the center of each grid cell instead of at the the intersection points of a finite difference grid. The Euler equations (2.0a) through (2.0d) take on a finite volume form[19] of

$$\frac{d}{dt}\left(S_{ij} w_{ij}\right) + Q_{ij} = 0 \qquad\qquad (3.0a)$$

where S_{ij} is the cell area, w_{ij} represents the conserved term, and Q_{ij} is the net flux out of the cell.

The flux term[19] can be evaluated at each cell as

$$Q_{ij} = \sum_{k=1}^{4} (\Delta y_k f_k - \Delta x_k g_k) \qquad (3.0b)$$

where f_k and g_k represent the flux vectors on the kth edge for the x and y directions respectively. The Δy and Δx are the increments of x and y along the edge of the cell, and the sum is over the four sides of the cell. The flux vectors[19] are taken as

$$f_2 = \frac{1}{2}(f_{i+1,j} + f_{i,j}) \qquad (3.0c)$$

where $f_{i+1,j}$ and $f_{i,j}$ are the flux values of the cells on either side of edge 2. This method reduces to a central difference scheme on a Cartesian grid. More detail discussion of the numerical methods employed in FLO52 may be found in Reference 19.

Upon initial inspection one would assume modification of the perfect gas to van der Waals equation of state to be a straightforward process; however, the perfect gas simplifications of the thermodynamic parameters are extensively embedded in most airfoil codes. The compressible gas relations used in FLO52 had to be developed for a van der Waals gas. The required van der Waals expressions for code modification were derived by applying the van der Waals equation of state, Equation (2.6), to the general expressions of the sound speed, internal energy, enthalpy, pressure, entropy, and the lift and drag coefficients; and then placed into equivalent expressions found in the FLO52 code. The

14

FLO52 airfoil code contained thermodynamic expressions for the perfect gas model of the form

$$P = P(e,\rho) \quad , \quad P = P(s,\rho)$$
$$e = e(P,\rho)$$
$$S = S(P,\rho) \tag{3.1}$$
$$a = a(P,\rho)$$

where the P is the pressure, e is the internal energy, a is the speed of sound, and ρ is the density. The entropy term is $S = \exp\left\{-\frac{(s-s_r)}{C_v}\right\}$. Therefore, the thermodynamic expressions with the van der Waals gas assumption were cast in the same manner.

Each expression was converted to the nondimensional form by

$$\bar{P} = \frac{P}{P_r}$$

$$\bar{\rho} = \frac{\rho}{\rho_r}$$

$$\bar{e} = \frac{e}{U_r^2}$$

$$\bar{\alpha} = \frac{\alpha \rho_r^2}{P_r} \tag{3.2a}$$

$$\bar{b} = b\rho_r$$

$$\bar{V} = \frac{V}{U_r}$$

$$H_0 = \frac{H_r}{U_r^2}$$

$$\bar{a}^2 = \frac{a^2}{U_r^2}$$

The reference values for Equations (3.2a) were taken to be:

$$U_r^2 = \frac{P_\infty}{\rho_\infty}$$

$$P_r = P_\infty$$

$$\rho_r = \rho_\infty \qquad\qquad\qquad (3.2b)$$

$$e_r = C_v T_r - \alpha \rho_r$$

$$H_r = H_\infty; \quad \text{where } H_\infty = h_\infty + \tfrac{1}{2} V_\infty^2$$

S_r was not needed explicitly because all entropy expressions are defined with the entropy term S ; and C_v is the constant volume specific heat.

The first pressure expression, $P = P(e,\rho)$, was obtained by integration of the general internal energy equation from Van Wylen and Sonntag[17]. The general form of the differential of the internal energy, e, expression is given in Equations (3.3).

$$de = C_v dT + \left[T \left(\frac{\partial P}{\partial T} \right)_v - P \right] dv \qquad (3.3a)$$

$$de = C_v dT + \left[P - T \left(\frac{\partial P}{\partial T} \right)_\rho \right] \frac{d\rho}{\rho^2} \qquad (3.3b)$$

Equation (3.3a) is the more common from of the generalized internal energy expression;

however, Equation (3.3b) was employed here. The partial derivative in Equation (3.3b),

$\left(\dfrac{\partial P}{\partial T}\right)_\rho$, was obtained by taking the partial derivative of the van der Waals Equation (2.6).

Substituting Equation (2.6) and

$$\left(\frac{\partial P}{\partial T}\right)_\rho = \frac{\rho R}{1-b\rho} \qquad (3.4)$$

in (3.3b) lead to

$$de = C_v dT - \alpha d\rho \cdot \qquad (3.5)$$

The specific heat C_v is take to be a constant. Integrating Equation (3.5) gave

$$\int_{e_r}^{e} de = C_v \int_{T_r}^{T} dT - \alpha \int_{\rho_r}^{\rho} d\rho$$

$$e - e_r = C_v \left(T - T_r\right) - \alpha \left(\rho - \rho_r\right) \qquad (3.6)$$

where C_v, α are assumed to be constant. Solving for temperature T led to

$$T = T_r + \frac{e - e_r + \alpha\left(\rho - \rho_r\right)}{C_v} \cdot \qquad (3.7)$$

Substituting Equation (3.7) into Equation (2.6) resulted in

$$P = \left[T_r + \frac{e - e_r + \alpha\left(\rho - \rho_r\right)}{C_v}\right] \frac{R\rho}{1-b\rho} - \alpha\rho^2 \cdot \qquad (3.8)$$

Elimination of the reference values T_r and e_r was accomplished by replacing e_r with the

expression $e_r = C_v T_r - \alpha \rho_r$ which lead to the pressure expression

$$P = \frac{R}{C_v} \frac{\rho(e + \alpha \rho)}{1 - b\rho} - \alpha \rho^2 = P(e, \rho) \ . \ (3.9)$$

Through the application of Equations (3.2a), the nondimensional form of Equation (3.9)

became

$$\bar{P} = \frac{R}{C_v} \frac{\bar{\rho}(\bar{e} + \bar{\alpha}\bar{\rho})}{1 - \bar{b}\bar{\rho}} - \bar{\alpha}\bar{\rho}^2 \ . \quad (3.10)$$

The internal energy expression as a function of pressure and density was found by solving

Equations (3.9) for e

$$e = \frac{\left(P + \alpha \rho^2\right)(1 - b\rho)}{\rho \dfrac{R}{C_v}} - \alpha \rho \quad (3.11)$$

where the nondimensional from is given by

$$\bar{e} = \frac{\left(\bar{P} + \bar{\alpha}\bar{\rho}^2\right)(1 - \bar{b}\bar{\rho})}{\bar{\rho} \dfrac{R}{C_v}} - \bar{\alpha}\bar{\rho} \ . \quad (3.12)$$

The entropy expression was derived from the general expression of

$$ds = C_v \frac{dT}{T} - \left(\frac{\partial P}{\partial T}\bigg|_v\right) dv \quad (3.13a)$$

18

$$ds = C_V \frac{dT}{T} - \left(\frac{\partial P}{\partial T}\bigg|_\rho\right)\frac{d\rho}{\rho^2} \qquad (3.13b)$$

from Van Wylen and Sonntag[17]. Substituting Equation (3.4) into Equation.(3.13.b) gave

$$ds = C_v \frac{dT}{T} - \left(\frac{R}{1-b\rho}\right)\frac{d\rho}{\rho} \cdot \qquad (3.14)$$

Integration of Equation (3.14) led to

$$s - s_r = C_V\left[\ell n(T) - \ell n(T_r)\right] - R\int_{\rho_r}^{\rho} \frac{d\rho}{\rho(1-b\rho)}$$

$$\frac{s-s_r}{C_V} = \ell n\left(\frac{T}{T_r}\right) + \frac{R}{C_V}\ell n\left[\left(\frac{1-b\rho}{\rho}\right)\left(\frac{\rho_r}{1-b\rho_r}\right)\right] \cdot \qquad (3.15)$$

If the exponential of both sides are taken, then we can write

$$\bar{S} = \exp\left(\frac{s-s_r}{C_V}\right) = \exp\left[\ell n\left\{\left(\frac{T}{T_r}\right)\left(\frac{1-b\rho}{\rho} \cdot \frac{\rho_r}{1-b\rho_r}\right)^{\frac{R}{C_V}}\right\}\right]$$

where C_V, R, and b, are taken to be constants.

The temperature T, and the reference temperature $T_r = T_\infty$ of Equation (3.15) were replaced with the following expressions:

$$T = \frac{(1-b\rho)(P+\alpha\rho^2)}{\rho R} \qquad (3.16)$$

$$T_\infty = \frac{(1-b\rho_\infty)(P_\infty + \alpha\rho_\infty^2)}{\rho_\infty R} \cdot \qquad (3.17)$$

19

Equations (3.16) and (3.17) were obtained by solving Equation (2.6) for the temperature. Substitution of Equations (3.16) and(3.17) into (3.15) yielded an intermediate form of the entropy expression given by

$$\exp\left(\frac{s-s_r}{C_v}\right) = \left\{\frac{(1-b\rho)(P+\alpha\rho^2)\rho_\infty}{\rho(1-b\rho_\infty)(P_\infty+\alpha\rho_\infty^2)}\right\}\left[\left(\frac{1-b\rho}{\rho}\right)\left(\frac{\rho_\infty}{1-b\rho_\infty}\right)\right]^{\frac{R}{C_v}} \bullet \quad (3.18)$$

The parameters of pressure , density, α, and b, were replaced with the appropriate expressions from Equations (3.2a). The final nondimensional expression for the entropy relation as a function of pressure and density is

$$\exp\left(\frac{s-s_r}{C_v}\right) = \left[\frac{1-\bar{b}\bar{\rho}}{(1-\bar{b})\bar{\rho}}\right]^{1+\frac{R}{C_v}} \times \left[\frac{\bar{P}+\bar{\alpha}\bar{\rho}^2}{1+\bar{\alpha}}\right] \quad (3.19)$$

and

$$\bar{S} = \exp\left(-\frac{(s-s_r)}{C_v}\right) = \left[\bar{\rho}\frac{(1-\bar{b})}{(1-\bar{b}\bar{\rho})}\right]^{1+\frac{R}{C_v}} \times \left[\frac{1+\bar{\alpha}}{\bar{P}+\bar{\alpha}\bar{\rho}^2}\right] \bullet \quad (3.20)$$

The other pressure relation required by the FLO52 is one which relates pressure as a function of the entropy expression S, and density, ρ. This expression is easily obtained from solving Equation (3.20) for pressure. The resulting pressure equation became

$$\bar{P} = \left[\left(\frac{1+\bar{\alpha}}{\bar{S}}\right)\left(\bar{\rho}\frac{1-\bar{b}}{1-\bar{b}\bar{\rho}}\right)^{1+\frac{R}{C_v}}\right] - \bar{\alpha}\bar{\rho}^2 \bullet \quad (3.21)$$

The last expression derived was for the speed of sound for a van der Waals fluid. The

20

general thermodynamic sound speed is

$$a^2 = \frac{\partial P}{\partial \rho}\bigg|_s \quad .$$

(3.22)

By expanding the derivative in Equation (3.22), the sound speed took the form of

$$a^2 = \frac{\partial P}{\partial \rho}\bigg|_s = -v^2\left[\left(\frac{\partial P}{\partial v}\right)_T + \left(\frac{\partial P}{\partial T}\right)_v\left(\frac{\partial T}{\partial v}\right)_s\right]$$

(3.23a)

and

$$\left(\frac{\partial T}{\partial v}\right)_s = -\left(\frac{\partial P}{\partial s}\right)_v$$

$$= -\left(\frac{\partial P}{\partial s}\right)_v\left(\frac{\partial s}{\partial T}\right)_v\left(\frac{\partial T}{\partial s}\right)_v$$

where $\left(\dfrac{\partial T}{\partial v}\right)_s = \dfrac{C_v}{T}$. Therefore, the sound speed became

$$a^2 = v^2\left[\frac{T}{C_v}\left(\frac{\partial P}{\partial T}\right)_v^2 - \left(\frac{\partial P}{\partial v}\right)_T\right] \quad .$$

(3.23b)

The derivatives

$$\left(\frac{\partial P}{\partial v}\bigg|_T\right) = -\frac{RT}{(v-b)^2} + \frac{\alpha}{v^3}$$

(3.24a)

$$\left(\frac{\partial P}{\partial T}\bigg|_v\right)^2 = \frac{R^2}{(v-b)^2}$$

(3.24b)

were obtained by differentiating the van der Waals equation (2.6). Substituting Equations

(3.24a) and (3.24b) into Equation (3.23b) resulted in

$$a^2 = \frac{RT}{(1-b\rho)^2}\left[1+\frac{R}{C_v}\right] - 2\alpha\rho \quad \bullet \qquad (3.25)$$

Replacing RT with

$$RT = \frac{(1-b\rho)\left(P+\alpha\rho^2\right)}{\rho} \qquad (3.26)$$

lead to the final form of the sound speed for a van der Waals fluid

$$a^2 = \left(\frac{P+\alpha\rho^2}{\rho(1-b\rho)}\right)\left(1+\frac{R}{C_v}\right) - 2\alpha\rho \quad \bullet \qquad (3.27)$$

The non-dimensional form Equation (3.27) is given by

$$\bar{a}^2 = \left(\frac{\bar{P}+\bar{\alpha}\bar{\rho}^2}{\bar{\rho}(1-\bar{b}\bar{\rho})}\right)\left(1+\frac{R}{C_v}\right) - 2\bar{\alpha}\bar{\rho} \quad \bullet \qquad (3.28)$$

The coefficients for lift and drag were obtained by integrating the pressure over the airfoil surface. The general form of the pressure coefficient is

$$C_p = \frac{P-P_\infty}{\frac{1}{2}\rho_\infty V_\infty^2} \qquad (3.29)$$

where C_p denotes the the general form of the pressure coefficient. In the original FLO52 code the pressure coefficient was defined specifically for the perfect gas. The FLO52

pressure coefficient was of the form

$$\bar{C}_p = \frac{\bar{P} - 1}{\frac{1}{2} \gamma M_\infty^2} \qquad (3.30)$$

where $\bar{C}_p$ represents the nondimensional pressure coefficient for a perfect gas, γ is

$$\left(1 + \frac{R}{C_v}\right).$$

If we let C_p' denotes the form of the pressure coefficient for the van der Waals gas, then

$$C_p' = \frac{\bar{P} - 1}{\frac{1}{2} M_\infty^2 \bar{a}_\infty^2} \qquad (3.31)$$

where $\bar{a}_\infty$ is the non-dimensional freestream sound speed for a van der Waals gas found to be

$$\bar{a}_\infty^2 = \frac{(1 + \bar{\alpha})\left(1 + \frac{R}{C_v}\right)}{(1 - \bar{b})} - 2\bar{\alpha} \quad \bullet \qquad (3.32)$$

Therefore we can write $C_p' = \bar{C}_p \frac{\gamma}{\bar{a}_\infty^2}$; and the correction factor for transforming the perfect

gas pressure coefficient, $\bar{C}_p$, to that of the van der Waals fluid is $\frac{\gamma}{\bar{a}_\infty^2}$.

23

The lift, drag, and pressure coefficients for the van der Waals fluid are related to the perfect gas versions in a similar manner by :

$$C_l' = \bar{C}_l \frac{\gamma}{\bar{a}_\infty^2}$$
(3.33)

$$C_d' = \bar{C}_d \frac{\gamma}{\bar{a}_\infty^2} \cdot$$
(3.34)

The relations derived in the above discussion are for FLO52 specifically; however, they should be applicable to other existing airfoil codes for two dimensional and steady state conditions. The version of FLO52 modified for a van der Waals fluid shall be referred to as the modified Euler code in order to avoid confusion when discussing the codes in subsequent sections.

Chapter 4

Results and Discussion

The modified Euler code, FLO52, was used to model various flow conditions for a NACA 0012 airfoil in a BZT fluid environment. In the following discussion of the results, all the studies were conducted for a NACA 0012 airfoil. Several thermodynamic states were chosen for the van der Waals fluid to illustrate the nonclassical and classical gas behavior. The results presented in this section attempt to illustrate the aerodynamic differences and advantages of the BZT fluid over the perfect gas. Critical Mach number predictions were made for the BZT fluid to define the freestream states which remain subsonic over the entire wing. Following the critical Mach number predictions are the analytical data generated by the modified Euler coded for both BZT and perfect gas fluids. These results support the critical Mach number predictions for BZT fluids, and give further evidence that these nonclassical gasdynamic fluid characteristics provide distinct advantages over the perfect gas. The unique characteristics of the BZT fluids were further examined by consideration of a high specific heat fluid which is subjected to various freestream thermodynamic conditions where the fluid transitions from the perfect gas behavior to that of the BZT fluid. Also, the dense gases which predict the existence of expansion shocks were investigated in this thesis.

In the subsequent discussion of the thesis results, all the data generated by the modified FLO52 code were determined to have reached convergence based upon several elements outlined below. Initial runs of the modified Euler code were made to predict perfect gas

behavior with the van der Waals equation of state. This was accomplished by setting the van der Waals coefficients to zero and the $R/C_v = 0.4$ to reproduce the results for air. The perfect gas simulation exercise provided an additional check on the validity of the modified FLO52 results. The results for the perfect gas cases compared well with other published results[19,20] as shown in Table 4.0. The surface plots for Mach number and pressure coefficient and the contour plots for Mach number were typical of perfect gas behavior for a NACA 0012 airfoil. The BZT fluid convergence criteria were also based upon the residual of the last iteration cycle, the number of iteration cycles, and the comparison of the analytical data for isentropic flow to the pressure and local Mach number predicted by the Bernoulli equation.

For the criteria of residual numbers, the maximum and average residual for each iteration cycle indicated the difference between data of a given cycle and that of the previous cycle. Residuals of the order of 10^{-3} are an indication that convergence has been achieved. In addition to small residual values, changes in the data due to increase in the number of iteration cycles were considered. Numerical data that has reached convergence will not change when the iteration cycle number is further increased. The BZT fluid test cases were run at 500, 1000, 1500, 2000, 2500, and 3500 cycles. Note that the multi-grid option in FLO52 was not used for generating the BZT fluid results; therefore, the cycle numbers are for a single grid numerical scheme. The results indicated that 2000 cycles were adequate for reaching a convergence condition for the BZT fluids. At the 2000 cycle condition the residuals were of the order of 10^{-4} to 10^{-3}. Also, the local pressure and Mach number results for isentropic flow conditions at 2000 cycles compared extremely well with the pressure and Mach numbers predicted by the Bernoulli equation as shown in Table 4.1. Equations (4.2), (4.3), (4.4) and (3.25) were used to make local Mach number and

26

pressure calculations where a freestream Mach number was assumed and the density was varied. In the calculations of local pressure and Mach numbers, Equation (4.4) was rearranged to solve for the local Mach number explicitly. Also, the stagnation conditions calculations were useful for checking the stagnation pressure calculated by the Euler code. The calculations of the stagnation pressure condition was obtained by setting the local Mach number in Equation (4.4) to zero and assuming a stagnation density value for $\bar{\rho} = \dfrac{\rho}{\rho_\infty}$.

BZT fluid critical Mach number calculations were made because the critical Mach number estimates are a simple means of predicting the transonic limits of a flow. By definition, the freestream Mach number at which the local Mach number first becomes sonic is the critical Mach number for that fluid and airfoil geometry. Because the maximum Mach number corresponds to the minimum pressure for the flow of interest, then we can say that the minimum pressure on the airfoil surface is equal to the pressure required to attain a local Mach number of one for the case of a critical Mach number flow. The minimum pressure coefficient on the airfoil is typically estimated from the Prandtl-Glauert equation

$$C_p\Big|_{min} = \frac{C_{p_{inc}}\Big|_{min}}{\sqrt{1 - M_\infty^2}} = f(M_\infty), \qquad (4.0)$$

for a fixed wing shape. The $C_p\Big|_{min}$ is the minimum pressure coefficient on the wing surface at a freestream Mach number of M_∞ . The $C_{p_{inc}}\Big|_{min}$ is the incompressible minimum pressure coefficient for a given airfoil geometry and fluid. The pressure

coefficient for a fluid may given by

$$C_p = \frac{\bar{P}-1}{\frac{1}{2}M_\infty^2 \bar{a}_\infty^2} = g(M_\infty, M) \cdot \qquad (4.1)$$

The expression for the pressure $\bar{P}$ is given by

$$\bar{P} = \left(\frac{T}{T_\infty}\right)\left(\frac{1}{Z_\infty}\right)\left(\frac{\bar{\rho}}{1-\bar{b}\bar{\rho}}\right) - \bar{\alpha}\bar{\rho}^2 \qquad (4.2)$$

where $Z_\infty = \dfrac{1}{(1+\bar{\alpha})(1+\bar{b})}$. Equation (4.2) was obtained by combining the van der Waals

equation of state (2.6), and the isentropic condition of

$$\frac{T}{T_\infty} = \left(\frac{1-\bar{b}}{1-\bar{b}\bar{\rho}}\right)^\delta (\bar{\rho})^\delta \qquad (4.3)$$

where $\delta = \dfrac{R}{C_v}$.

The critical Mach number was calculated from the Bernoulli equation

$$M_\infty^2 = \frac{2}{\delta \bar{a}_\infty^2 Z_\infty}\left\{\left(\frac{T}{T_\infty}\right)\left\{1+\frac{\delta}{1-\bar{b}\bar{\rho}}\right\} - \left(1+\frac{\delta}{1-\bar{b}}\right)\right\}$$

$$-\frac{4\bar{\alpha}}{\bar{a}_\infty^2}\{\bar{\rho}-1\} + \frac{\bar{a}^2}{\bar{a}_\infty^2}M^2 \qquad (4.4)$$

where the freestream speed of sound was obtained by evaluating Equation (3.25) at
freestream conditions.

28

Therefore, the critical Mach number estimation is the freestream Mach number which satisfies

$$f(M_\infty) = g(M_\infty, M = 1) \qquad (4.5)$$

Equation (4.5) may be solved graphically by plotting $g(M_\infty, M = 1)$ which is represented by Figure 4.0, curve (1), for a perfect gas. Curve (2) of Figure 4.0 represents the Prandtl-Glauert equation of (4.0). The intersection of curve (1) and (2) is the solution to equation (4.5). The curves of Figure 4.0 were found by the parametric solution for Equation (4.0) and (4.1). Solutions to Equation (4.0) were obtained by varying the freestream Mach number for a given $C_{p_{inc}}\big|_{min}$ value. The $C_{p_{inc}}\big|_{min}$ was calculated by the Euler code for the NACA 0012 airfoil at zero angle of attack. The parametric solutions for Equation (4.1) was found by setting the local Mach number to 1 in Equation (4.4) and varying the density term, $\bar{\rho} = \dfrac{\rho}{\rho_\infty}$, in Equations (4.2),(4.3),(4.4), and (3.25). The detail derivation of Equations (4.2) through (4.4) may be found in Appendix A.

The potential advantages of the BZT fluids may first be recognized from the critical Mach number curves shown in Figure 4.1. Figure 4.1 represents the critical Mach number curves for the perfect gas fluid and a van der Waals fluid at specific volume ratios of $v/v_c = \{3.03, 2.0, 1.429, 1.25\}$. In all BZT fluid cases the pressure ratio was taken to be $P/P_c = 1.0$, and the specific heat term was assumed to be $R/C_v = 0.02$. Figure 4.1 shows that the critical Mach numbers increase as the fluid approaches the dense gas states. This initial study indicates that the BZT fluids may allow much higher freestream fluid velocity

conditions and higher angles of attack for a given airfoil than predicted for the perfect gas. The critical Mach number study is only a crude estimate of the BZT fluid capabilities. To further substantiate the BZT fluid characteristics, the modified Euler code was used to predict the flow field for a NACA 0012 air foil.

The first results from the modified FLO52 code were for a freestream Mach number of $M_\infty = 0.8$ with a NACA 0012 airfoil, and angles of attack of 0 to 6 degrees. These results were compared to perfect gas predictions under the same freestream conditions and airfoil geometry. The comparison of the BZT fluids to the perfect gas clearly defines the advantages of the BZT fluids over the perfect gas . The thermodynamic state of the van der Waals gas was chosen to be at a specific volume ratio of $v_\infty/v_c = 1.25$ and pressure ratio of $P_\infty/P_c = 1.0$ which is a point in the single phase vapor region near the saturation curve and critical pressure, and well within the region of nonclassical fluid behavior (i.e. negative Γ). The specific heat term $R/C_v = 0.02$ roughly corresponds to the case of normal decane (n- $C_{10}H_{22}$). This gave van der Waals coefficients for $\bar{\alpha}$, and $\bar{b}$ of 1.92, and 0.267 respectively. The specifications for the perfect gas runs were for a $R/C_v = 0.02$ which gave a typical perfect gas ratio of specific heats, C_p/C_v, value of 1.02.

Figures 4.2a, 4.3a, and 4.4a, are the surface plots of the pressure coefficient and local Mach number for the BZT fluids at free stream condition of $M_\infty = 0.8$. The plots show how the flow near the airfoil changes due to the increase in angle of attack from 0 to 6 degrees. Even at an angle of attack of 6 degrees, the flow appears to be only slightly sonic. In contrast the surface plots for the perfect gas in Figure 4.2b indicate massive compression shocks for an angle of attack of 0° at a freestream Mach number of 0.8. At increasing angles of attack for a perfect gas fluid, the shocks become increasingly

30

stronger. For an angle of attack of 6 degrees, the maximum local Mach number has reached 1.5 as shown in Figure 4.4b.

The differences between the BZT fluid and perfect gas are further illustrated by Figures 4.5 to 4.6. The lift and drag curves for both the BZT fluid and the perfect gas are predicted by the Euler equations. Therefore, no boundary layer effects such as boundary layer separation are accounted for in the lift and drag results. Figure 4.5a show that the lift coefficients for the perfect gas are greater than the BZT fluids for a Mach number of 0.8. However, the BZT fluid lift coefficient curve for $M_\infty = 0.92$ is greater than for perfect gas as shown in Figure 4.6a. The wave drag coefficient plots of Figures 4.5b, 4.5c, 4.6b, and 4.6c, further support the reduction or elimination of kinetic energy losses due to shocks for the BZT fluids. The wave drag curve for the BZT fluid lies close to zero whereas the perfect gas curve increases sharply for the entire range of angles of attack in Figures 4.5b and 4.6b. Because the BZT fluid flow is subsonic for the flow conditions of Figures 4.5 and 4.6, the low wave drag coefficients are likely due to numerical errors which result from large gradients at the leading and/or trailing edges . The wave drag plots of figures 4.5c and 4.6c reflect a substantial reduction of the wave drag for the BZT fluid over the perfect gas. The wave drag is also a measure of the strength of the shocks. The actual drag is expected to be even stronger due to shock induced separation which is expected to occur in actual flows. The BZT fluids are capable of sustaining subsonic, and therefore shock-free, flow at much higher angles of attack than for perfect gas fluids.

The corresponding contour plots at $M_\infty = 0.8$ and the angle of attack ranges from $0°$ to $6°$ for BZT fluids and perfect gas of Figures 4.7 to 4.9 further support the nonclassical gasdynamics predictions of previous investigations. The classical gasdynamic behavior of

the perfect gas is observed in Figure 4.7b. The sonic contour region of Figure 4.7b, referred to often as the sonic bubble, is located on the wing surface over the maximum wing thickness. The resulting compression shock is located downstream of the maximum wing thickness. Both the sonic bubble and the compression shock location are typical of the perfect gas and agrees well with results of published literature[19,20]. All perfect gases will behave in a manner similar to that seen in Figure 4.7b. That is the sonic bubble and compression shock will be located in relatively the same location for a given wing surface. For the BZT fluids, none of the contour plots of Figures 4.7a and 4.8a gave indications that a sonic region existed on the wing surface. The Mach number contour plot for an angle of attack of 6° shows a very small region of sonic flow in Figure 4.9a. Figure 4.10 depicts a more severe flow environment in which $M_{\infty} = 0.92$ and the angle of attack of is 4 degrees. Even in this case the sonic bubble is only slightly larger. The sonic regions of Figures 4.9a and 4.10 are located near the leading edge of the airfoils as opposed to sonic region location predicted by the perfect gas theory. Also, there is no indication of a compression shock in Figure 4.10. Therefore, the Euler code results indicate that BZT fluids significantly delay supersonic flow. This conclusion is in agreement with predictions by Thompson[4], and the critical Mach number estimates presented earlier in this chapter.

The BZT fluid surface and contour plots also indicate the existence of a phenomenon referred to as Mach number oscillations[21]. The local Mach number for a BZT fluid may decrease and increase while the corresponding density is increasing monotonically. That is a Mach number versus density curve may contain local minimums and maximums as shown in Figure 4.11. The detailed arguments leading to Figure 4.11 are found in Reference 21. This phenomenon does not exist for the perfect gas because the perfect gas

theory indicates that the local Mach number will decrease monotonically as density increases. Figure 4.11 is a qualitative BZT fluid plot of M versus ρ for various stagnation density conditions indicated on the $M = 0$ line. The $J = 0$ curve of Figure 4.11 is the locus of all maximum and minimum points for the M vs ρ curves. The nonclassical gasdynamic region is inside the $J = 0$ curve where $J > 0$. Curves such as a, b, and c, represent high stagnation density conditions and contain discrete sections which are located in the $J > 0$ region. Therefore, curves a, b, and c, contain a local maximum and minimum. In a perfect gas, $J < 0$ and $\dfrac{\rho \Gamma}{a} > 1$ is true everywhere. Thus the ρ_l^1 to ρ_r^1 and $J > 0$ region shrinks to zero. Figure 4.12 is a BZT fluid plot of M, ρ versus Cartesian X axis of the computational grid as predicted by the Euler code. The X values are grid Cartesian coordinates normalized by the airfoil length. The airfoil surface data lies between X values of 0.0 and 1.0. The minimum values of the Mach number curve located near the X= 0.0 and X=1.0, correspond to the leading and trailing edges of the airfoil. The regions of local Mach number maxima correspond to monotonically increasing density values. Figure 4.12 most closely resembles curve c of Figure 4.11 where the curve is subsonic in the region near the local Mach number maximum.

The surface and contour plots give further support to the prediction of oscillating Mach numbers for BZT fluids. For perfect gas fluids, the Mach number and negative pressure coefficient surface plots have a one to one correspondence. That is, given a Mach number surface plot, one can easily predict the the pressure coefficient variation on the airfoil surface. This local Mach number to pressure relationship no longer is true for BZT fluids as shown by the surface plots of Figures 4.2a, 4.3a, and 4.4a. The surface plots of Figures 4.2a, 4.3a, and 4.4a contain local Mach number maximums at the leading and

trailing edge of the airfoil. These Mach number maxima correspond to the maxima of Figure 4.11. The Mach number contour plots of Figures 4.7a, 4.8a, 4.9a, and 4.10, show multiple contour regions for the a given Mach number value at both the leading and trailing edges. The corresponding pressure contours indicate monotonically increasing pressure contours at the leading edge and monotonically decreasing pressure contours at the trailing edge. Thus, the oscillating Mach number phenomenon is another significant difference between the BZT fluid and perfect gas.

The gasdynamic characteristics of high specific heat fluid (i.e., $C_v/R \geq 50$) which is modeled with the van der Waals equation of state may assimilate fluid behavior from perfect gas to BZT fluids when subjected to the appropriate undisturbed thermodynamic conditions. Figure 4.13 is for a perfect gas with an ideal gas specific heat ratio of 1.02. Figures 4.14, 4.15, and 4.16, depict the gasdynamic trends of the high specific heat fluid defined by $C_v/R=50$, $Z_c=0.375$, $P_\infty/P_c=1.0$, and v_∞/v_c over the range of 1.25 to 3.03.

Figure 4.14 is the surface for the undisturbed thermodynamic state of $v_\infty/v_c=3.03$, and $P_\infty/P_c=1.0$ at zero degree angle of attack and freestream Mach number of 0.8. Figure 4.14 compares well with the perfect gas of Figure 4.13 because the thermodynamic state of $v_\infty/v_c=3.03$, and $P_\infty/P_c=1.0$ is near the perfect gas regime. A region of supersonic flow exists over the wing surface of Figure 4.14, and resembles the perfect gas predictions of Figure 4.13. In Figure 4.15, the undisturbed thermodynamic state of $v_\infty/v_c=2.0$ and $P_\infty/P_c=1.0$ is moving away from the perfect gas regime toward the BZT fluid condition. Figure 4.15 still contains a supersonic region; however the number of grid points which are supersonic are much less than shown in Figure 4.14. The high specific heat fluid subjected to the undisturbed thermodynamic state of $v_\infty/v_c=1.25$ and $P_\infty/P_c=1.0$ is shown in Figure

4.16. The supersonic region and consequently the compression shock seen in the previous figures are nonexistent in Figure 4.16. The freestream thermodynamic state is located near the saturated vapor curve and critical pressure region (i.e. negative Γ region) and hence shows marked contrast with the perfect gas theory.

Other interesting results from this dense gas investigation are shown in Figure 4.17 which predicts the existence of both compression and expansion shocks in the flow. Figure 4.17 reveals a small region of sonic and supersonic flow near the trailing edge of the wing. As a result, a compression shock is generated in order to decelerate the flow to stagnation conditions. An expansion shock is observed in the region at the leading edge. This conclusion is based upon the decrease in pressure indicated by the pressure coefficient curve. Figure 4.18 is the corresponding Mach number contour plots for the expansion shock case. Figure 4.18 is also a good example of the Mach number oscillation phenomenon where double sonic contours occur at the leading and trailing edges of the airfoil. Again the results support the theoretical prediction of the existence of expansion shocks for BZT fluids. All the results to date indicate the existence of expansion shocks are accompanied by a trailing edge compression shock. It is of interest to ask whether a thermodynamic state and Mach number combination may exist which would result in a flow involving only expansion shocks. Future work which investigates the existence of a flow with only expansion shocks would be a valuable contribution in the study of dense fluids for aerodynamic applications.

The thesis results support the conclusions from the BZT fluid theory which predicts that a high specific heat fluid must have freestream thermodynamic conditions in the dense gas region (i.e. near the saturated vapor curve and in the vicinity of the critical pressure) in

order to exhibit nonclassical gasdynamic characteristics. The results also serve to further confirm the validity of the modified FLO52 code data since the code predicts behavior similar to that of the perfect gas for the $v_-/v_c = 3.03$ and BZT behavior for the $v_-/v_c = 1.25$.

The advantage of the BZT fluids over those of the perfect gas is in the area of extended subsonic flow for as high an angle of attack as 6°. A turbine blade ordinarily experiences a wide range of fluid velocities from an inlet conditions of M=0.6 to an outlet condition of 1.5; therefore, turbine blades are subjected to strong shock environments when the working fluid behaves as a perfect gas. The surface plots for the BZT fluids indicated a shock free environment up to an angle of attack of 6.0 degrees at a freestream Mach number of 0.8. Therefore, the energy losses resulting from shocks can be greatly reduced for a turbine or perhaps even eliminated through the application of the BZT fluid as the turbomachinery working fluid. In addition adverse pressure gradients due to compression shocks result in shock-induced boundary layer separation. The elimination of shock waves, particularly compression shocks, will eliminate this loss mechanism.

Chapter 5

Conclusions and Recommendations

This thesis is an important first step in the investigation of dense gases as practical working fluids for turbomachinery. The modified Euler code results indicate that the BZT fluids significantly delay supersonic flow over a NACA 0012 airfoil as compared to the predictions for the perfect gas theory. Drastic reduction in drag for the dense gases over perfect gas was observed. The dense gases were shown to behave as perfect gases at low density conditions; however, as the freestream density value was increased from $\rho_\infty = 0.33\rho_c$ to $\rho_\infty = 0.8\rho_c$ the fluid behaved as a BZT fluid. The Euler code results for BZT fluids also indicated the existence of expansion shocks accompanied by weak compression shocks on the leading and trailing edges of the wing, respectively.

The study revealed numerous advantages of BZT fluids. The shock free or weak shock environment of the BZT fluids allows turbine blades to sustain high freestream Mach number flows at high angles of attack without the detrimental effects of strong compression shocks. In addition the high angles of attack may extend the stall limit of the turbine blades; and therefore, extend the operating range of turbines. The BZT fluid results from this thesis supports many of the predictions made from the previous investigations.

More studies must be conducted before all the feasibility issues are answered for BZT fluid technology. More real fluids need to be investigated for BZT fluid characteristic potentials so that a broader range of working fluids are available. Currently there is little experimental

data for BZT fluids. Experimental data for BZT fluids need to be obtained to verify existing analytical predictions and to uncover feasibility issues which have not been anticipated. Experimental efforts could begin with employing a shadowgraph or schlieren flow visualization technique for observing shock waves in a BZT fluid at subcritical freestream Mach numbers.

References

1.   Bethe, H.A., "The theory of shock waves for an aribitrary equation of state", Office of Scientific Research and Development, Report No. 545, 1942.

2.   Zel'dovich, Y. B., "On the possibility of rarefaction shock waves", *Zh. Eksp. Teor. Fiz.*,1946, pp. 363-364.

3.   Zel'dovich, Y. B., and Raizer, Y. P., *Physics of shock Waves and High Temperature Hydrodynamic Phenomena*, Academic, New York, 1966.

4.   Thompson, P. A., "A Fundametal Derivative in Gasdynamics", The Physics of Fluids, Vol. 14, 1971, pp.1843-1849.

5.   Lambrakis, K. C., and Thompson, P.A., "Existence of Real Fluids with a Negative Fundamental Derivative Γ ", The Physics of Fluids, Vol.15, 1972, pp. 933-935.

6.   Thompson, P.A., and Lambrakis, K. C.,"Negative shock waves", Journal of Fluid Mechanics, Vol. 60, 1973, pp. 187-208.

7.   Cramer, M.S.,and Kluwick, A., "On the propagation of waves exhibiting both positive and negative nonlinearity", Journal of Fluid Mechanics, Vol. 142, 1984, pp. 9-37.

8.   Cramer, M.S., and Kluwick, A., and Watson, L.T., and Pelz, W., "Dissipative waves in fluids having both positive and negative nonlinearity", Journal of Fluid Mechanics, Vol. 169, 1986, pp. 323-336.

9.   Cramer, M.S., and Sen, R., "Exact solutions for sonic shocks in van der Waals gases", The Physics of Fluids, Vol. 30, 1987, pp. 377-385.

10.   Cramer, M.S., and Sen, R., "Shock formation in fluids having embedded regions of negative nonlinearity", The Physics of Fluids, Vol. 29, 1986, pp. 2181-2191.

11.   Cramer, M.S., "Dynamics of shock waves in gases having large specific heats", Proceedings of the 20th Midwestern Mechanics Conference, Purdue University, 1987.

12.   Cramer, M. S., "Structure of weak shocks in fluids having embedded regions of negative nonlinearity", The Physics of Fluids, Vol. 30, 1987, pp. 3034-3044.

13.   Cramer, M.S., " Shock splitting in single-phase gases", Journal of Fluid Mechanics, Vol. 199, 1989, pp. 281-296.

14. John, J.E.A., *Gasdynamics*, Allyn and Bacon, Inc., 1978.

15. Anderson Jr., J.D., *Fundamental of Aerodynamics*, McGraw Hill Book Company, 1984.

16. Bertin, J.J., and Smith, M. L., *Aerodynamics for Engineers*, Prentice-Hall, Inc., 1979.

17. Van Wylen, G.J., and Sonntag, R.E., *Fundamentals of Classical Thermodynamics*, John Wiley and Sons, Inc., Copyright 1973.

18. Cramer, M.S., "Negative nonlinearity in selected fluorocarbons", The Physics of Fluids, Vol. 1, 1989, pp. 1894-1897.

19. Jameson, A. and Yoon, S. "Multigrid Solution of the Euler Equations Using Implicit Schemes", AIAA Journal, Vol. 24, 1986, pp.1737-1743.

20. Dadone, A., and Moretti, G., "Fast Euler Solver for Transonic Airfoils Part II: Applications", AIAA Journal, Vol. 26, 1988, pp. 417-424

21. Cramer, M. S., "Nonclassical Dynamics of Classical Gases", Lecture Series for International Center of Mechanical Sciences, Udine, Italy, 1989.

Table 2.0 Negative Γ fluids calculations from the Martin-Hou equation of state. Each fluid was found to have a region of negative nonlinearity in the single-phase region. The last column gives the minimum values of $\rho\Gamma/a$ on the critical isotherm (Reference 18).

Fluid	$\dfrac{C_{v_-}(T_c)}{R}$	T_c	P_c	Z_c	$\left.\dfrac{\rho\Gamma}{a}\right|_{T_c}$
$C_{10}F_{22}$	74.8	578	12.9	0.255	0.04
$C_{10}F_{18}$(PP5)	64.5	565.2	17.3	0.262	0.11
$C_{11}F_{20}$(PP9)	72.8	586.6	16.4	0.261	0.05
$C_{13}F_{22}$(PP10)	78.4	632.2	16.0	0.283	-0.08
$C_{14}F_{24}$(PP11)	97.3	650.2	14.4	0.269	-0.15
$C_{16}F_{26}$(PP24)	112.0	701.2	15.1	0.289	-0.36
$C_{17}F_{30}$(PP25)	123.0	687.3	10.9	0.239	-0.22
$C_{12}F_{27}$N(FC-43)	93.0	567.2	11.2	0.260	-0.03
$C_{15}F_{33}$N(FC-70)	118.7	608.2	10.2	0.270	-0.17
$C_{18}F_{39}$N(FC-71)	145.0	646.2	9.3	0.275	-0.29
$C_{11}F_{23}HO_3$	82.9	536	10.7	0.254	0.10
$C_{14}F_{29}HO_4$	109.0	568	8.3	0.245	-0.02
$C_{17}F_{35}HO_5$	135.7	595	7.6	0.239	-0.11

Table 4.0 Comparison of the Euler code data with published data for lift and drag coefficients.

Case	Lift Coefficient	Drag Coefficient
$M_\infty = 0.8$, $\alpha = 0°$, $\gamma = 1.4$		
Euler Code	0.0	0.0091
Dadone & Moretti[20]	0.0	0.0071
Jameson & Yoon[19]	0.0	0.0086
$M_\infty = 0.8$, $\alpha = 1.25°$, $\gamma = 1.4$		
Euler Code	0.3454	0.0228
Dadone & Moretti[20]	0.3750	0.0229
Jameson & Yoon[19]	0.3513	0.0230
$M_\infty = 0.85$, $\alpha = 0°$, $\gamma = 1.4$		
Euler Code	0.0	0.0454
Dadone & Moretti[20]	0.0	0.0431
Jameson & Yoon[19]	0.0	0.0471
$M_\infty = 0.85$, $\alpha = 1°$, $\gamma = 1.4$		
Euler Code	0.3116	0.0536
Dadone & Moretti[20]	0.3610	0.0522
Jameson & Yoon[19]	_____	_____

Table 4.1 Comparison of Bernoulli's equation calculations and Euler code data of local Mach number and pressure values at freestream conditions of $M_\infty = 0.92$, $v_\infty = 1.11 v_c$, $P_\infty = 1.08 P_c$, and $R/C_v = 0.02$.

Density	Mach No. Bernoulli Equation	Pressure Bernoulli Equation	Mach No. Euler code	Pressure Euler code
1.2638	0.4506	1.0701	0.4512	1.0701
1.2284	0.5425	1.0577	0.5416	1.0577
1.1994	0.6131	1.0487	0.6125	1.0487
1.1601	0.7026	1.0378	0.7019	1.0378
1.1049	0.8088	1.0241	0.8080	1.0241
1.0286	0.9022	1.0066	0.9010	1.0066
0.9999	0.9204	1.00	0.9198	1.000
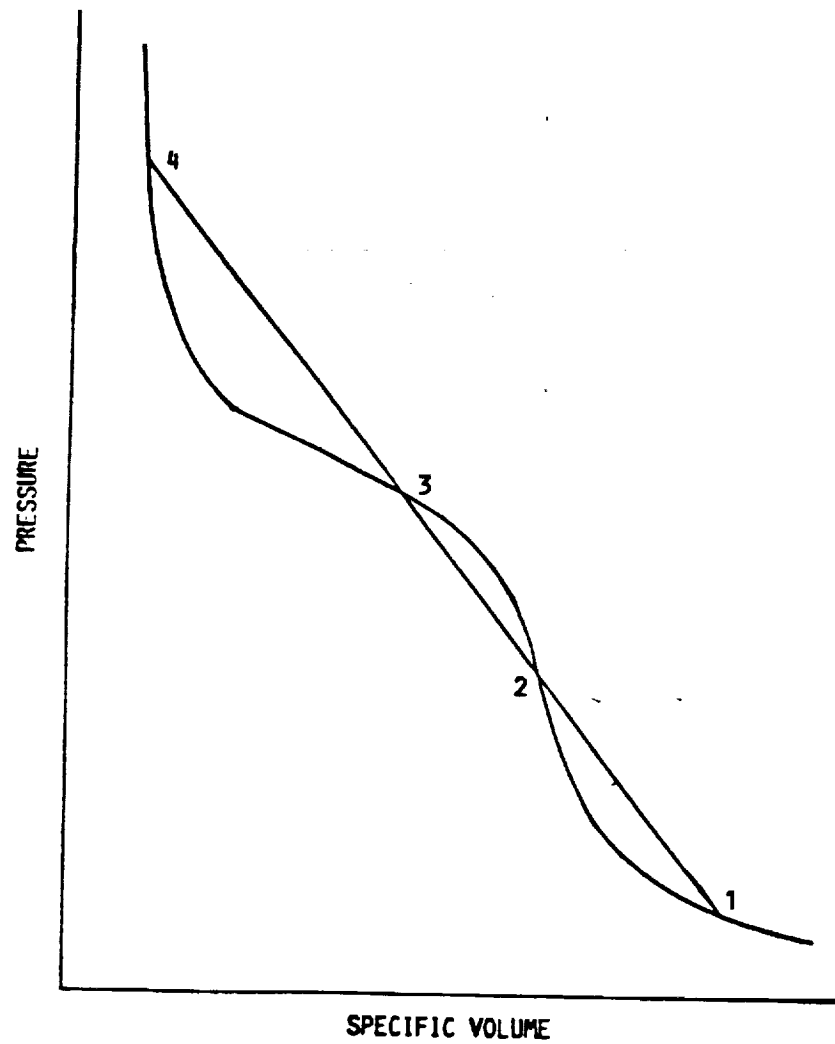
Figure 2.0. Shock adiabat going through the $\Gamma < 0$ region.
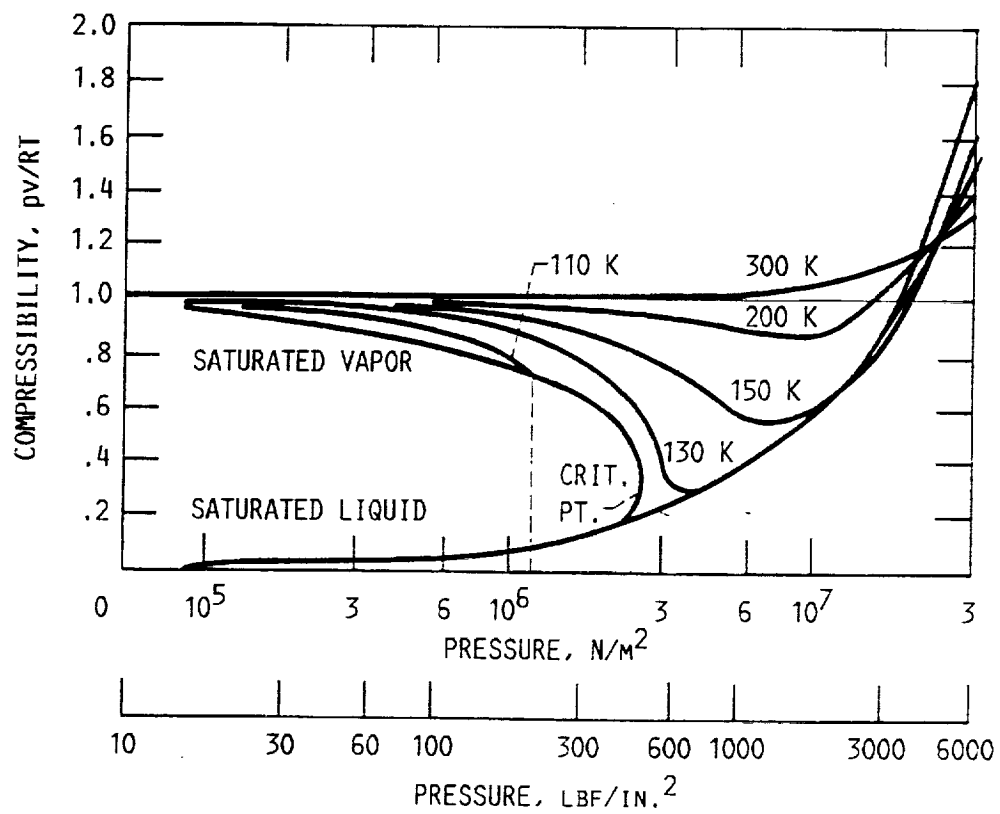
Figure 2.1. Compressibility chart for Nitrogen (Reference 17).
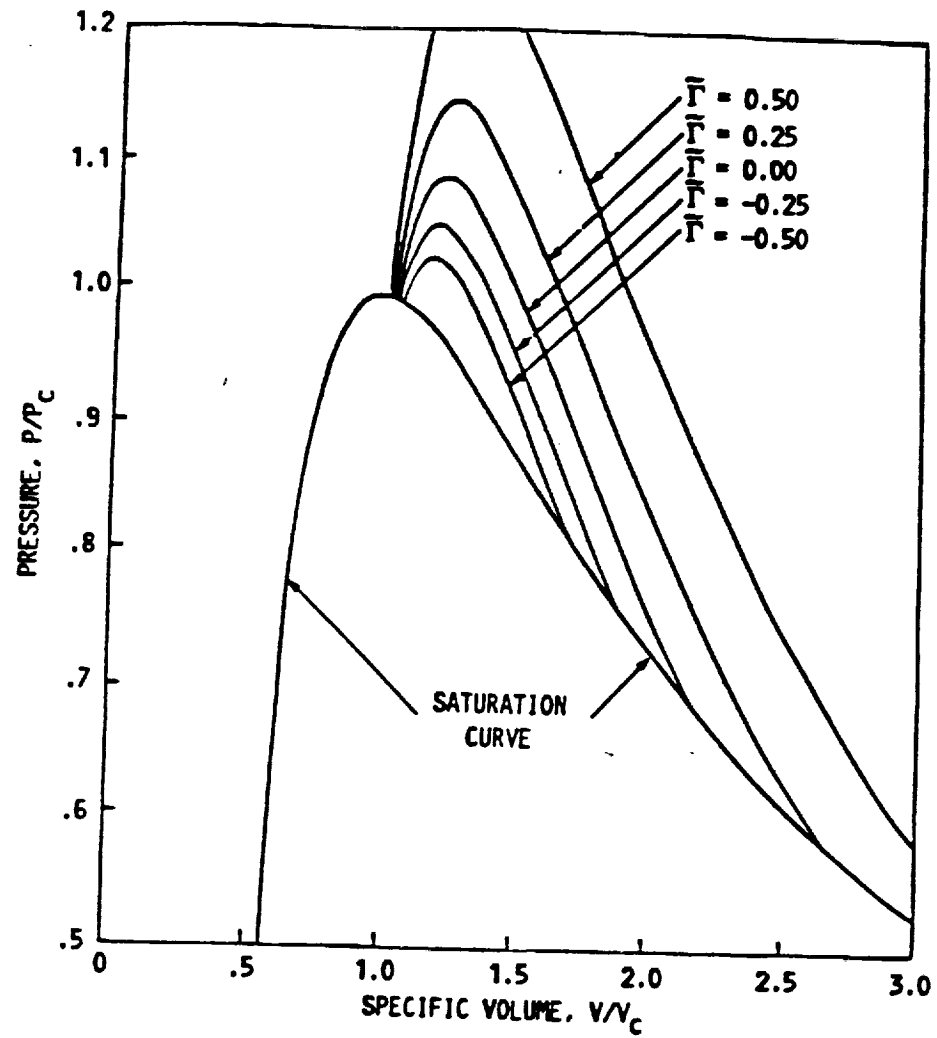
Figure 2.2. Constant $\bar{\Gamma} = \rho\Gamma/a$ contours for a van der Waals gas with $C_v/R=50$. The subscript c denotes conditions at the thermodynamic critical point (Reference 10).

46
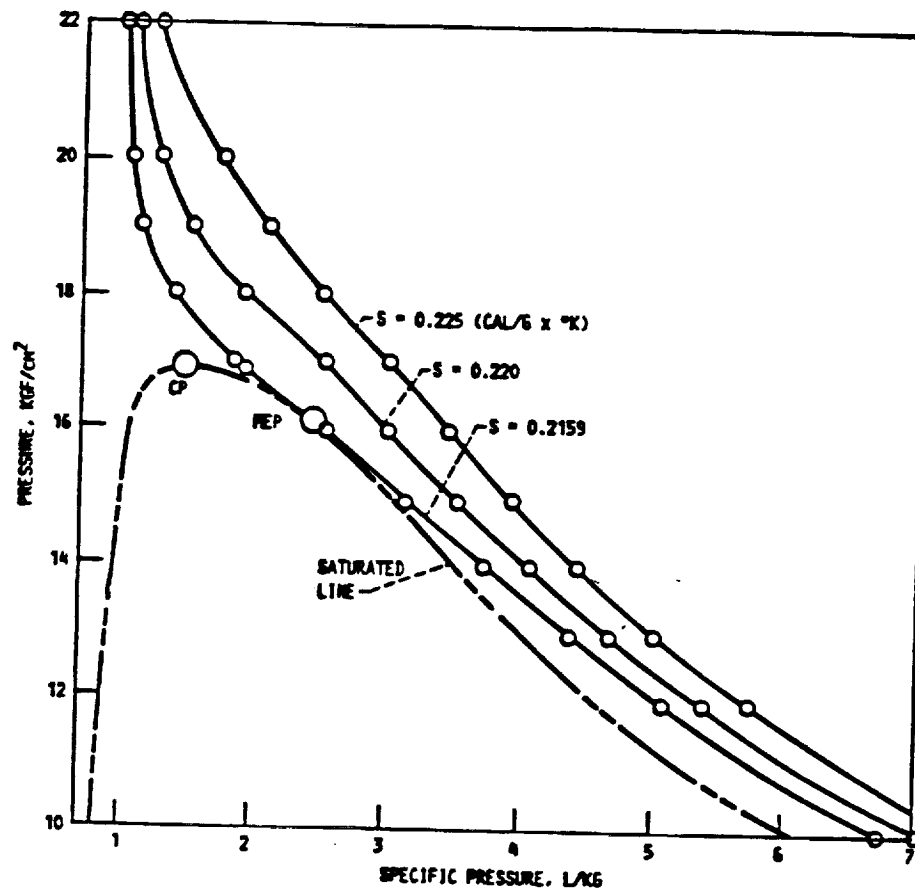
Figure 2.3. Isentropes in the Pv plane for perfluoromethyldecalin (Reference 5).
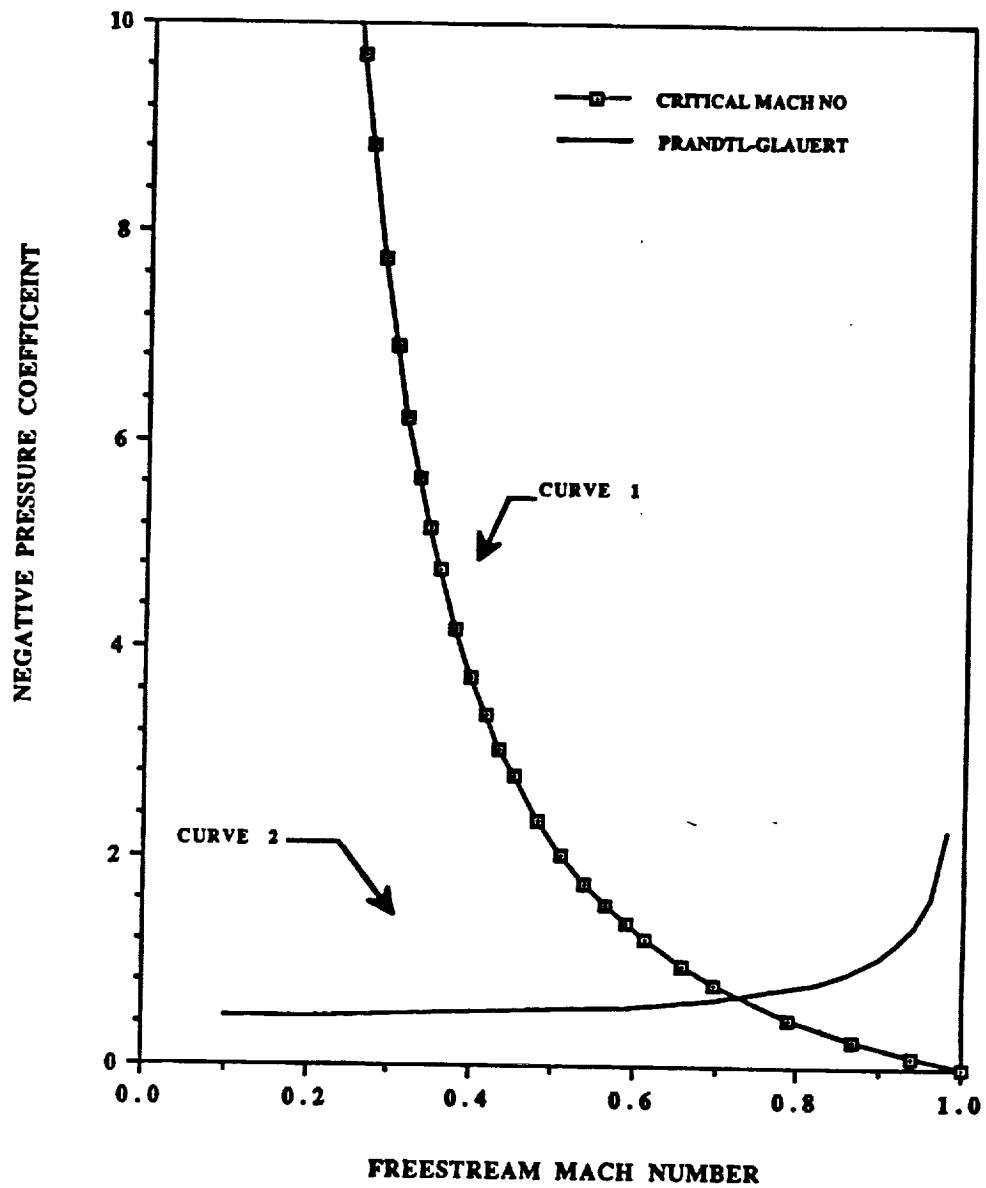
Figure 4.0. Perfect gas critical Mach number estimates for a NACA 0012 airfoil at 0.0 degree angle of attack.
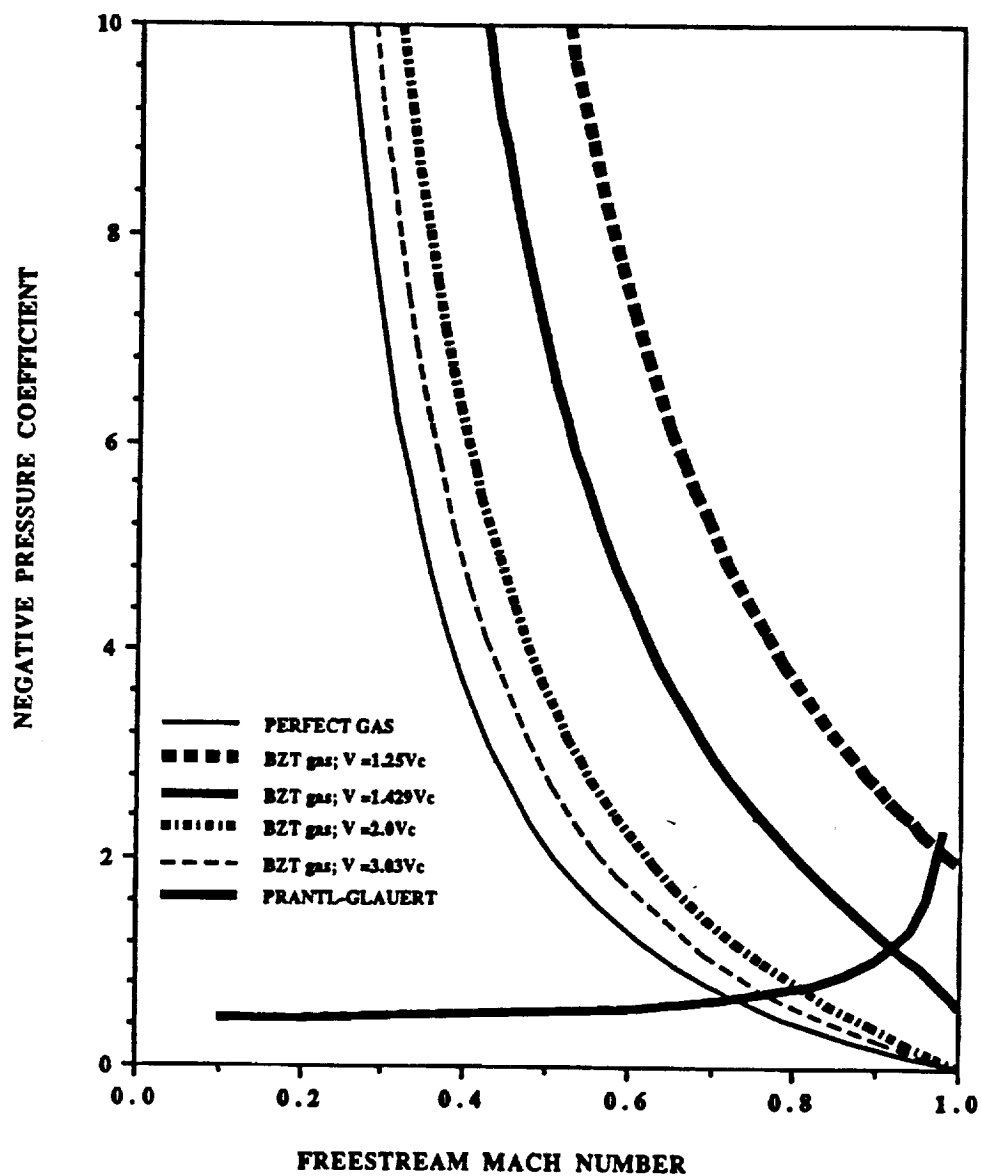
Figure 4.1. Critical Mach number estimates for the perfect gas and BZT fluids, and for the NACA 0012 airfoil at zero angle of attack.
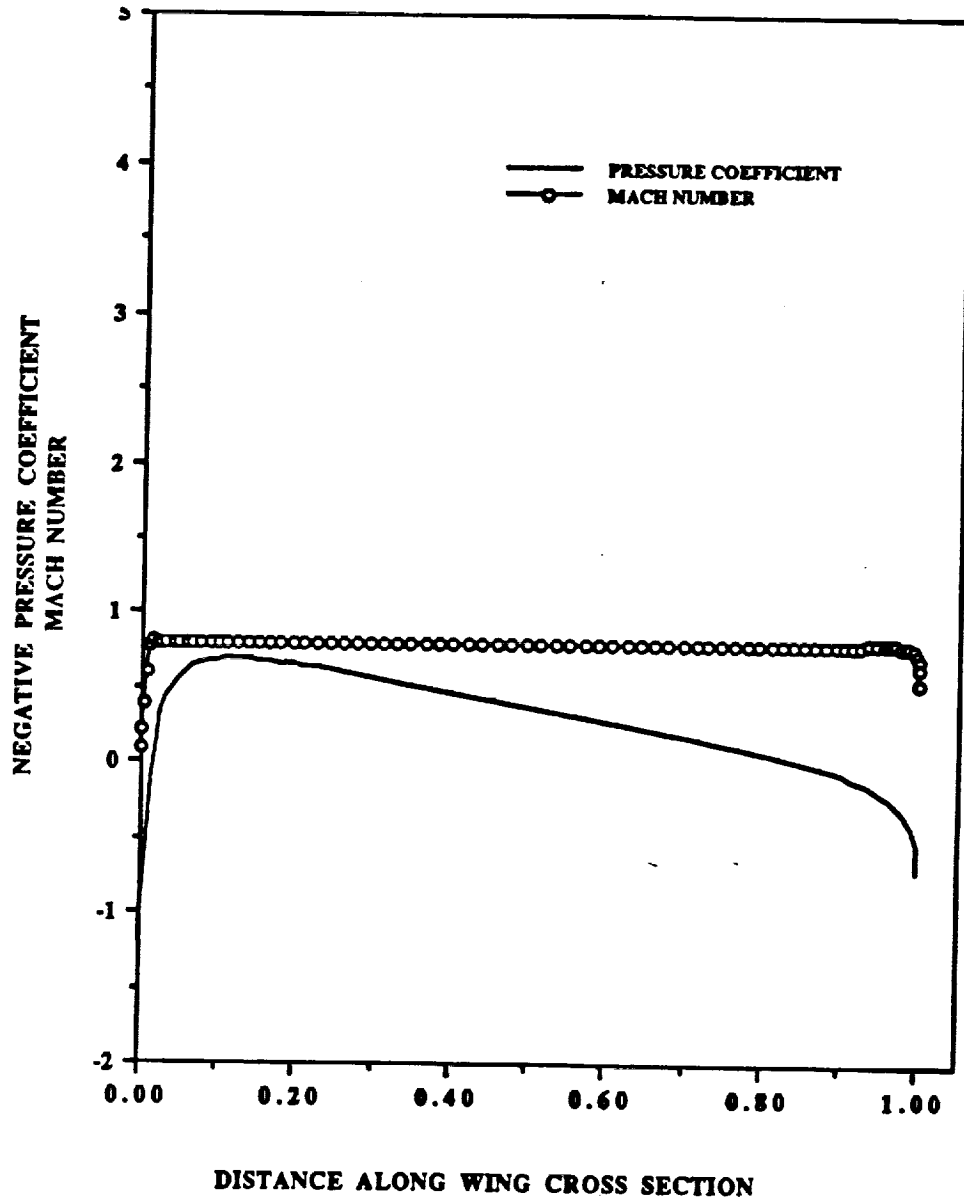
Figure 4.2a. BZT fluid surface plots of negative pressure coefficient and local Mach number for a NACA 0012 airfoil at freestream conditions of $M_\infty = 0.8$, angle of attack of 0.0 degree. The fluid is at conditions of $V_\infty = 1.25 V_c$, $P_\infty = 1.0 P_c$, and has a specific heat value of $R/C_v = 0.02$.

50
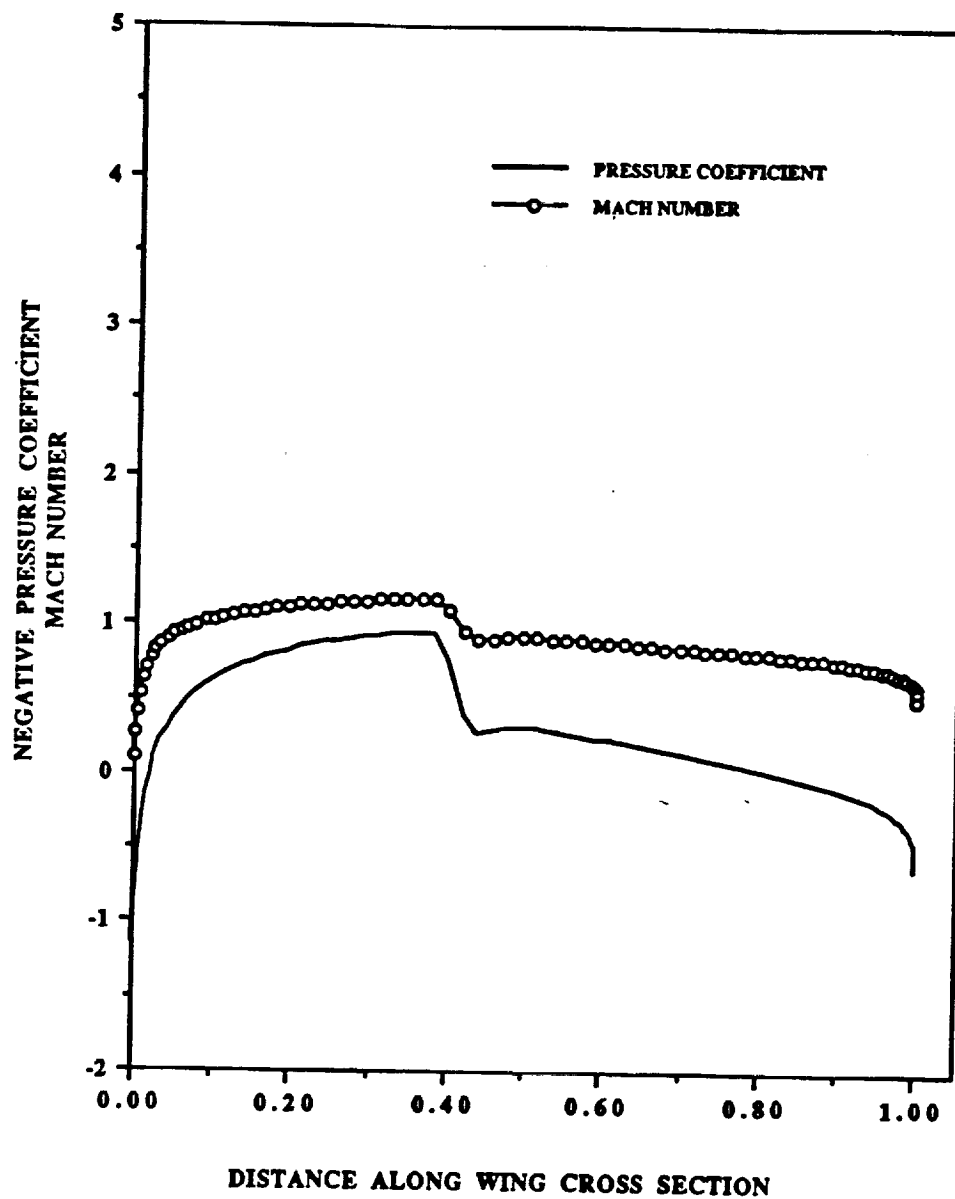
Figure 4.2b. Perfect gas surface plots of negative pressure coefficient and local Mach number for a NACA 0012 airfoil at $M_\infty = 0.8$, angle of attack of 0.0 degree. The fluid has a specific heat value of $R/C_v = 0.02$.
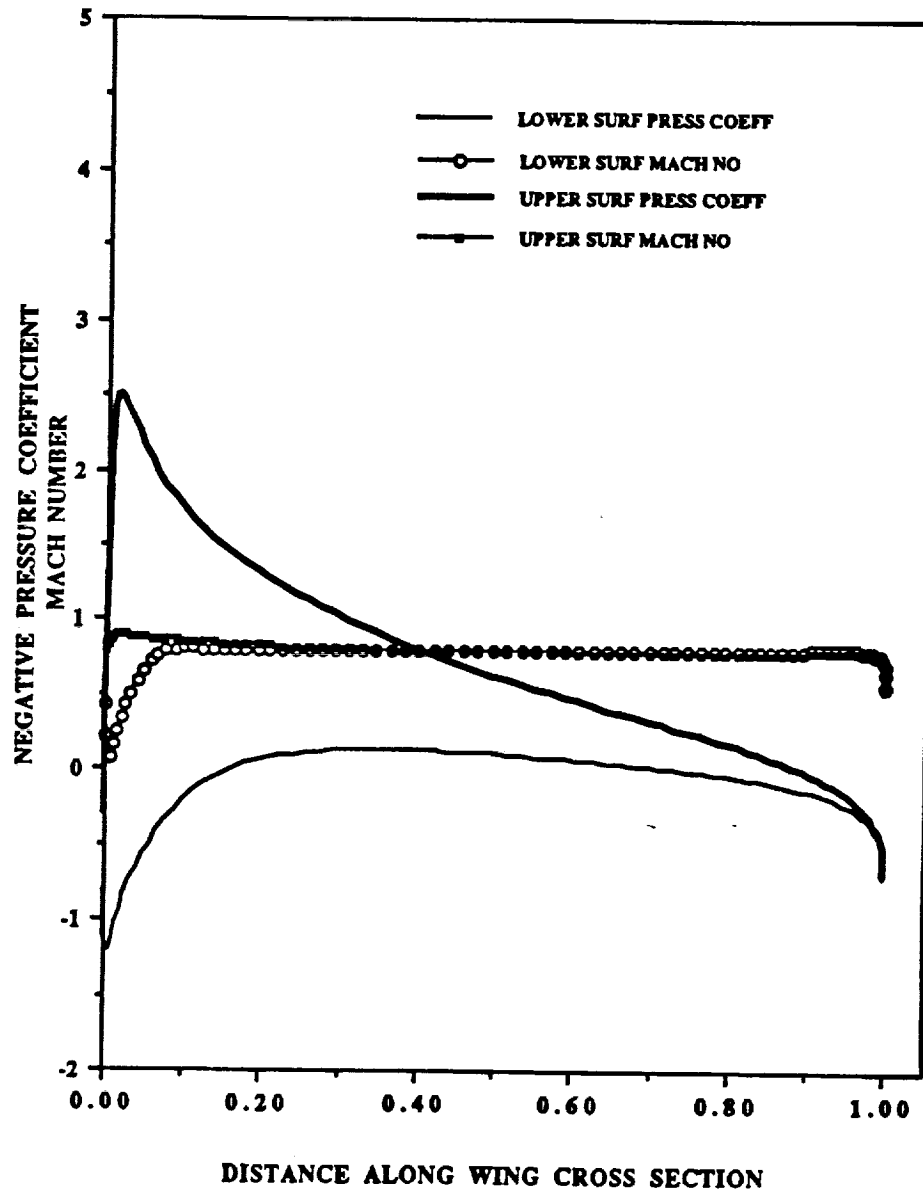
Figure 4.3a. BZT fluid surface plots of negative pressure coefficient and local Mach number for a NACA 0012 airfoil at freestream conditions of $M_\infty = 0.8$, angle of attack of 4.0 degrees. The fluid is at conditions of $V_\infty = 1.25V_c$, $P_\infty = 1.0P_c$, and has a specific heat value of $R/C_v = 0.02$.
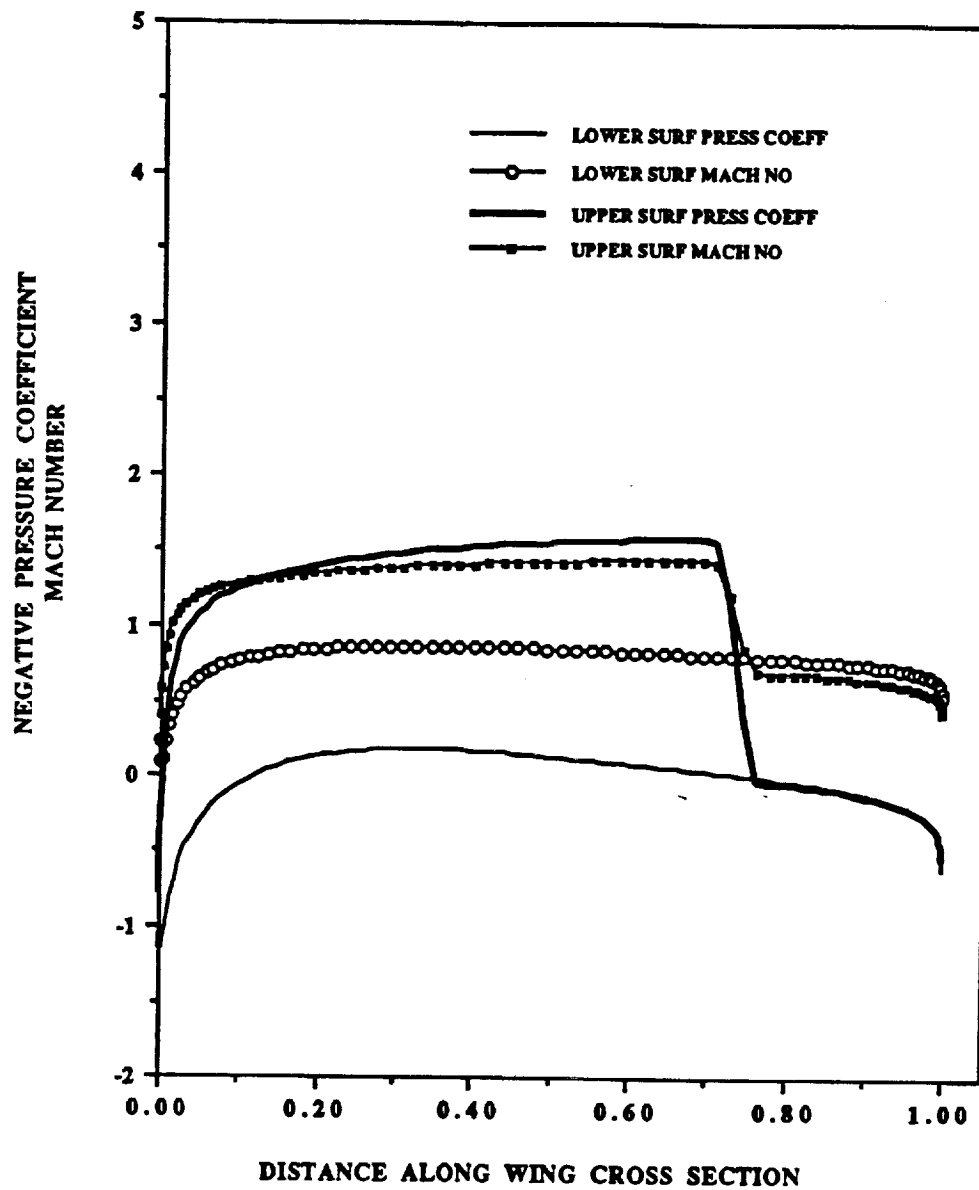
Figure 4.3b. Perfect gas surface plots of negative pressure coefficient and local Mach number for a NACA 0012 airfoil at $M_\infty = 0.8$, and an angle of attack of 4.0 degrees. The specific heat value of the fluid is $R/C_v = 0.02$.
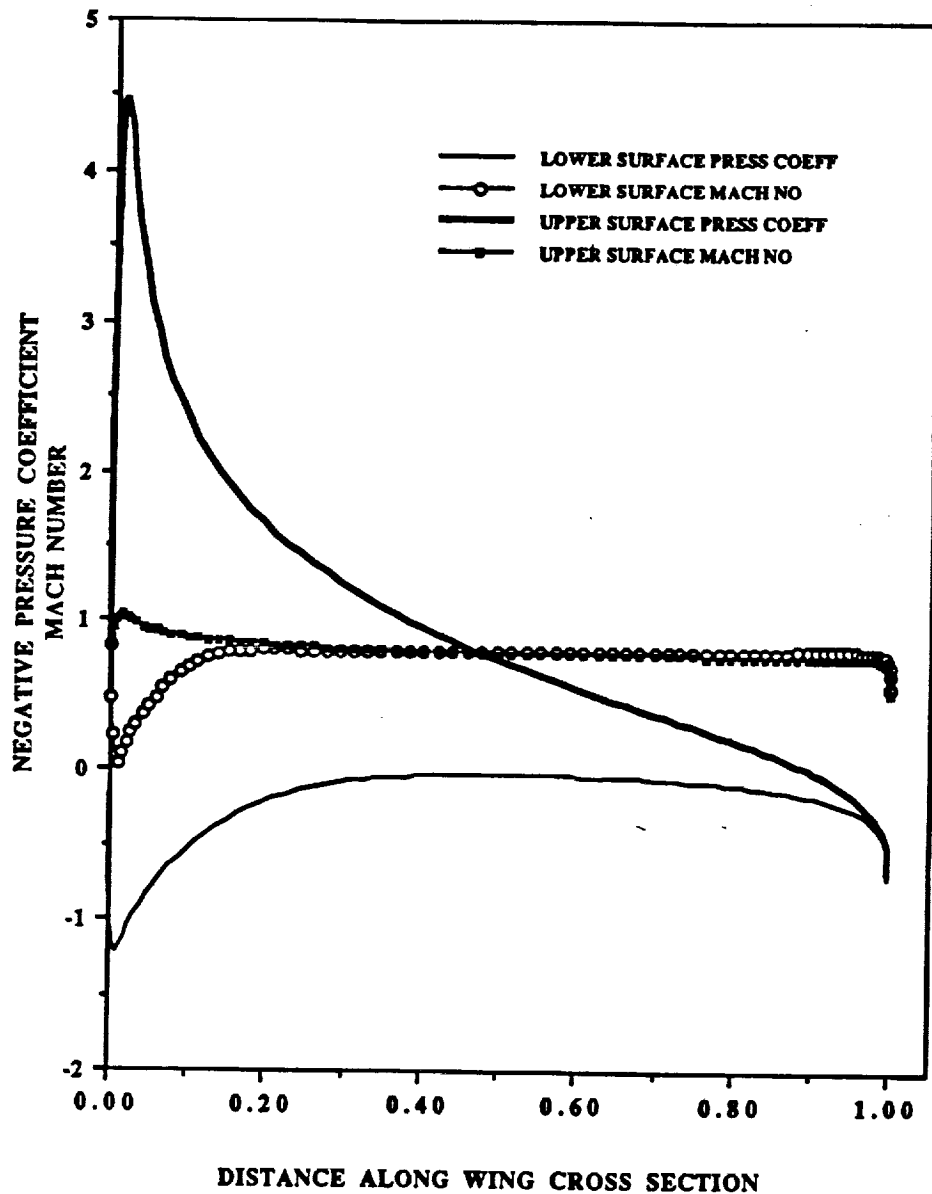
Figure 4.4a. BZT fluid surface plots of negative pressure coefficient and local Mach number for a NACA 0012 airfoil at freestream conditions of $M_\infty = 0.8$, and an angle of attack of 6.0 degrees. The fluid is at conditions of $V_\infty = 1.25 V_c$, $P_\infty = 1.0 P_c$, and has a specific heat value of $R/C_v = 0.02$.
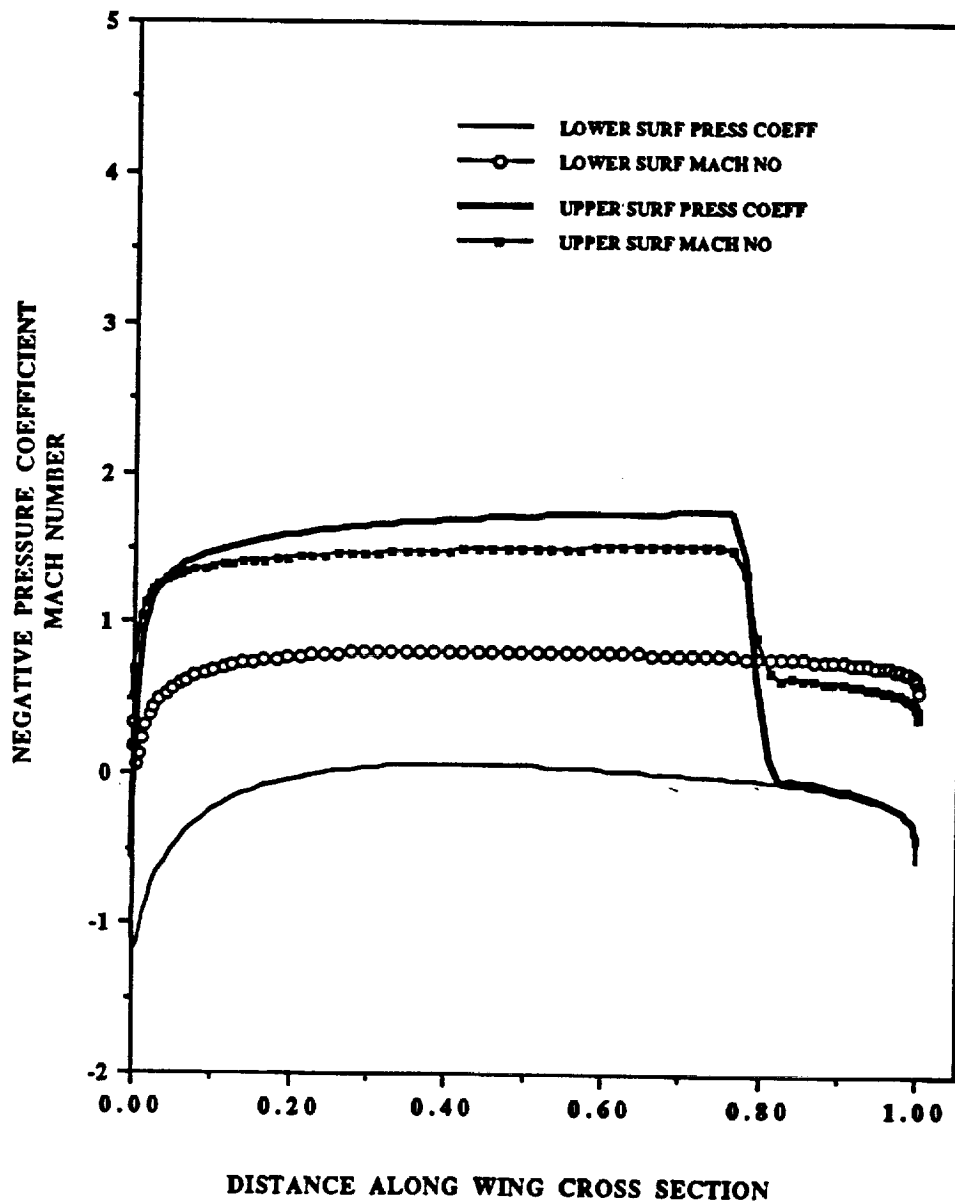
Figure 4.4b. Perfect gas surface plots of negative pressure coefficient and local Mach number for a NACA 0012 airfoil at $M_\infty = 0.8$, angle of attack of 6.0 degrees. The fluid has a specific heat value of $R/C_v = 0.02$.
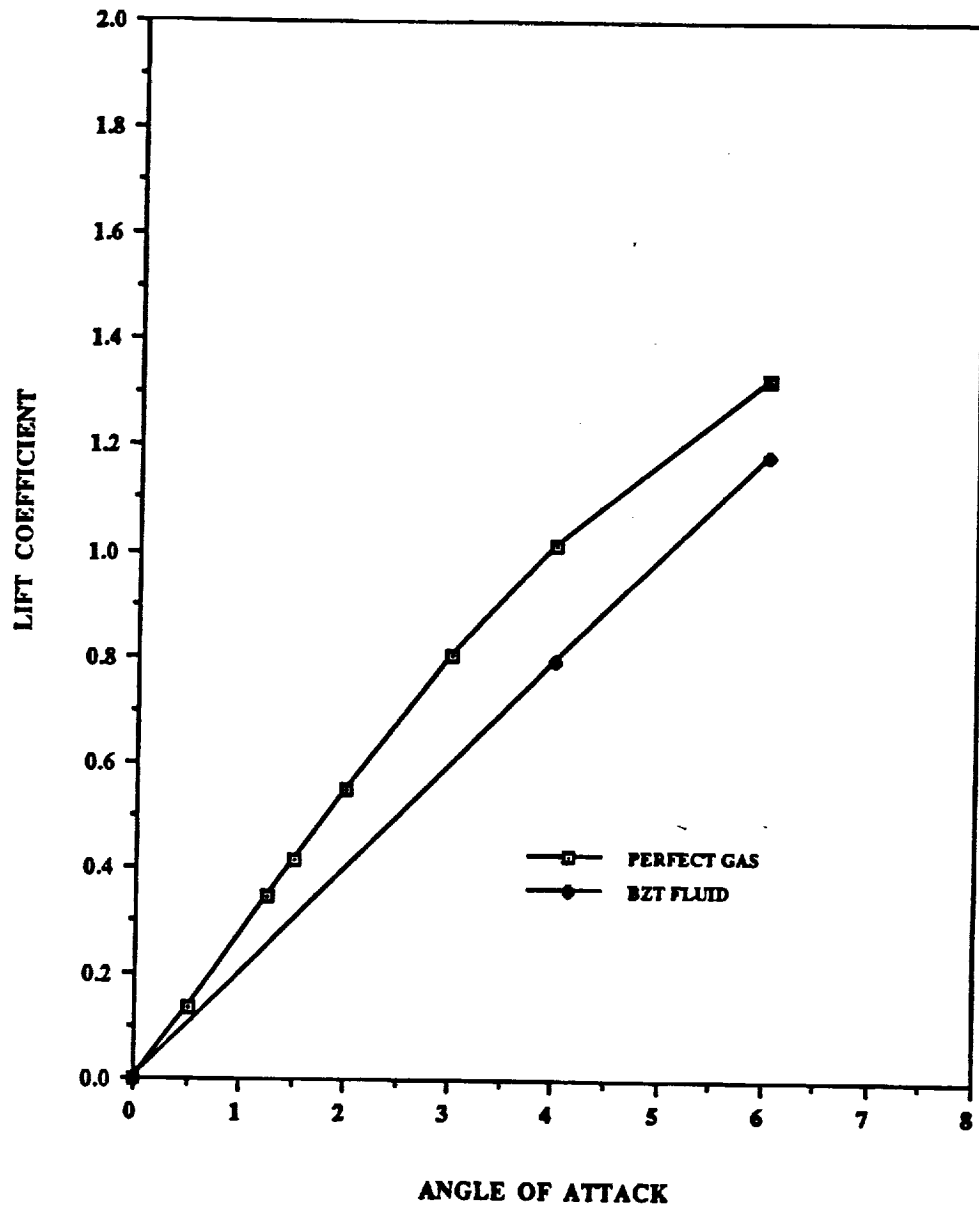
Figure 4.5a. BZT fluid and perfect gas lift coefficient versus angle of attack for a NACA 0012 airfoil at $M_\infty = 0.8$, and angle of attack range of 0.0 to 6.0 degrees. Both fluids have specific heat values of $R/C_v = 0.02$.
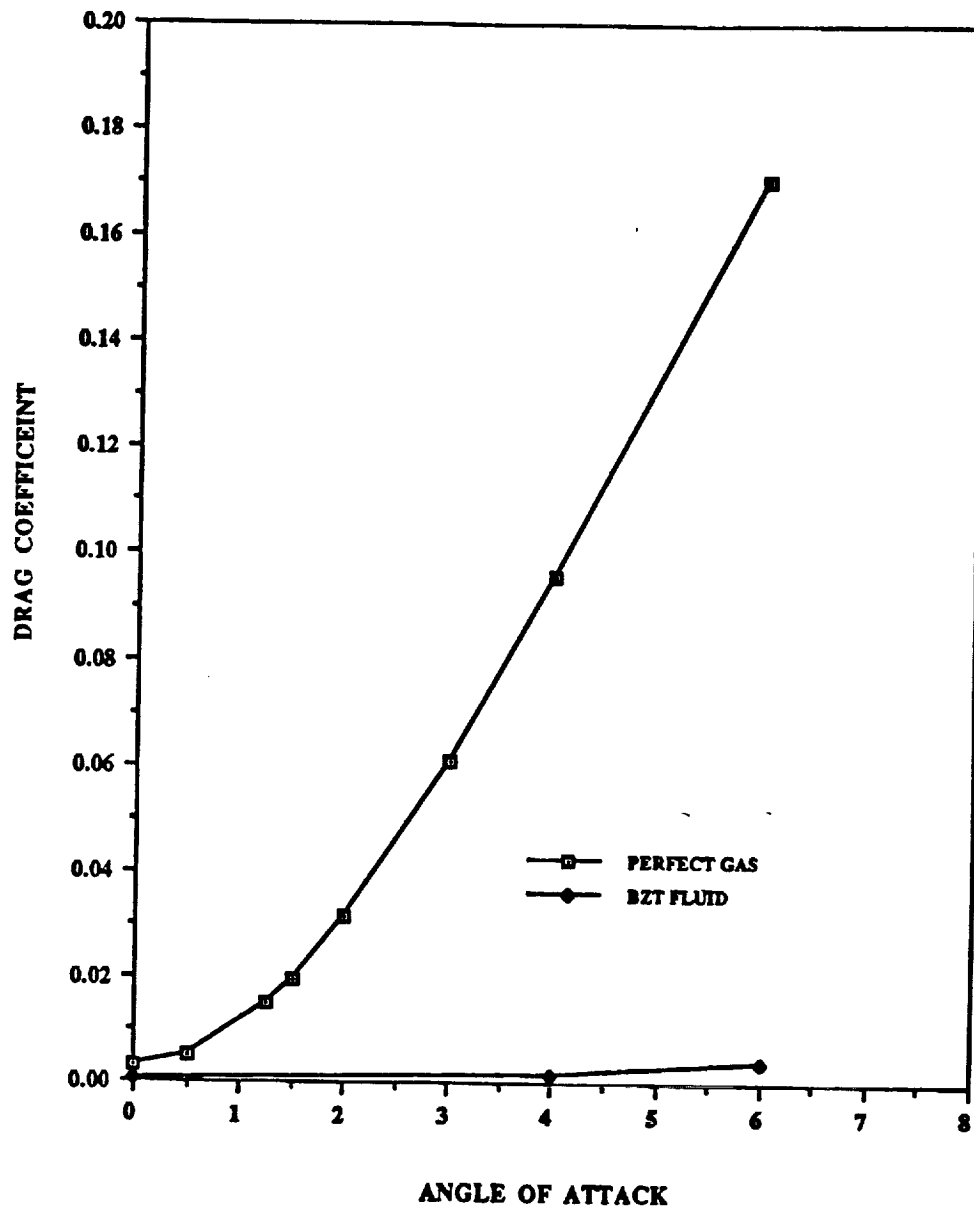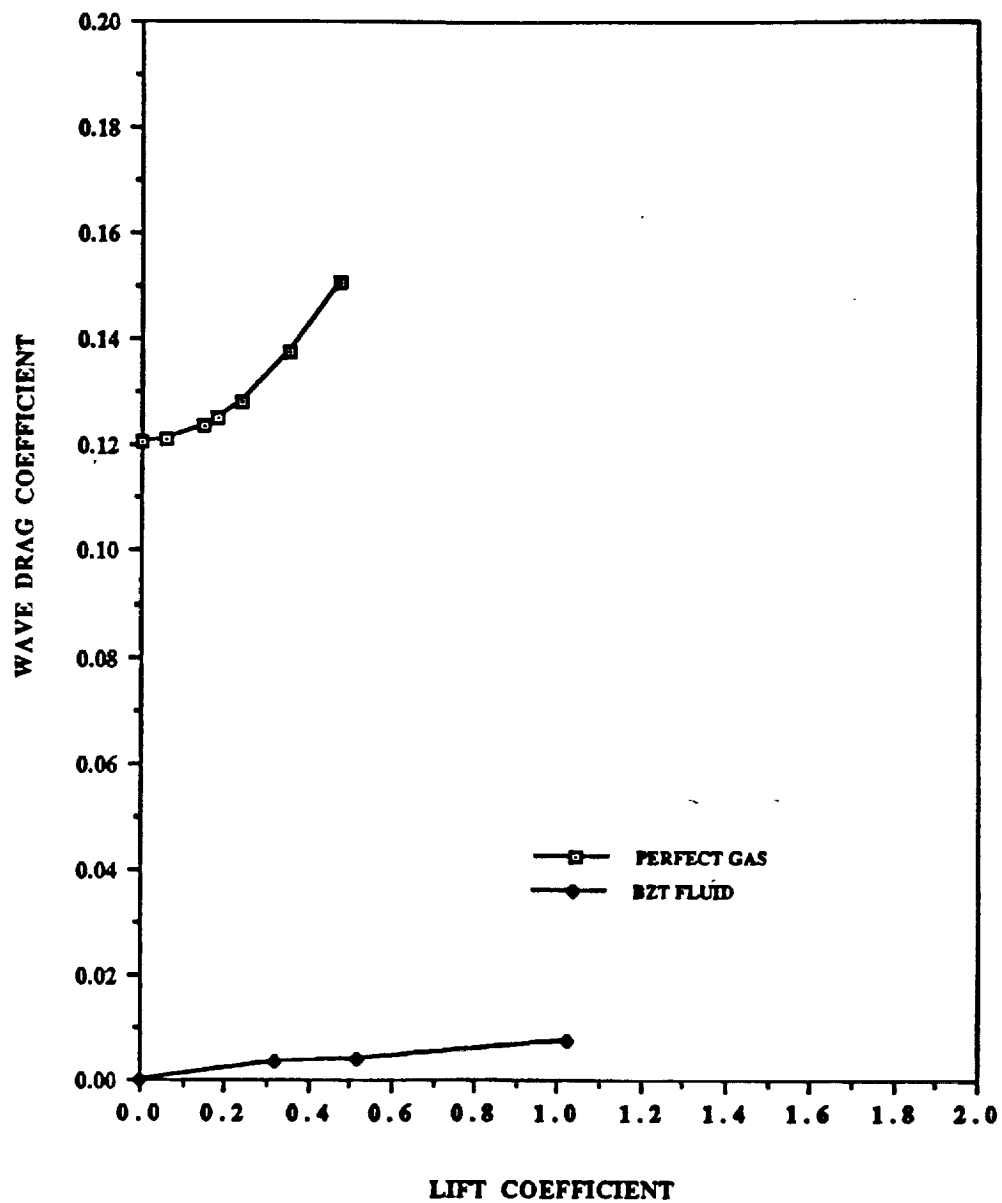
Figure 4.5b. BZT fluid and perfect gas drag coefficient versus angle of attack for NACA 0012 airfoil at $M_\infty = 0.8$, and angle of attack range of 0.0 to 6.0 degrees. Both fluids have specific heat values of $R/C_v = 0.02$.
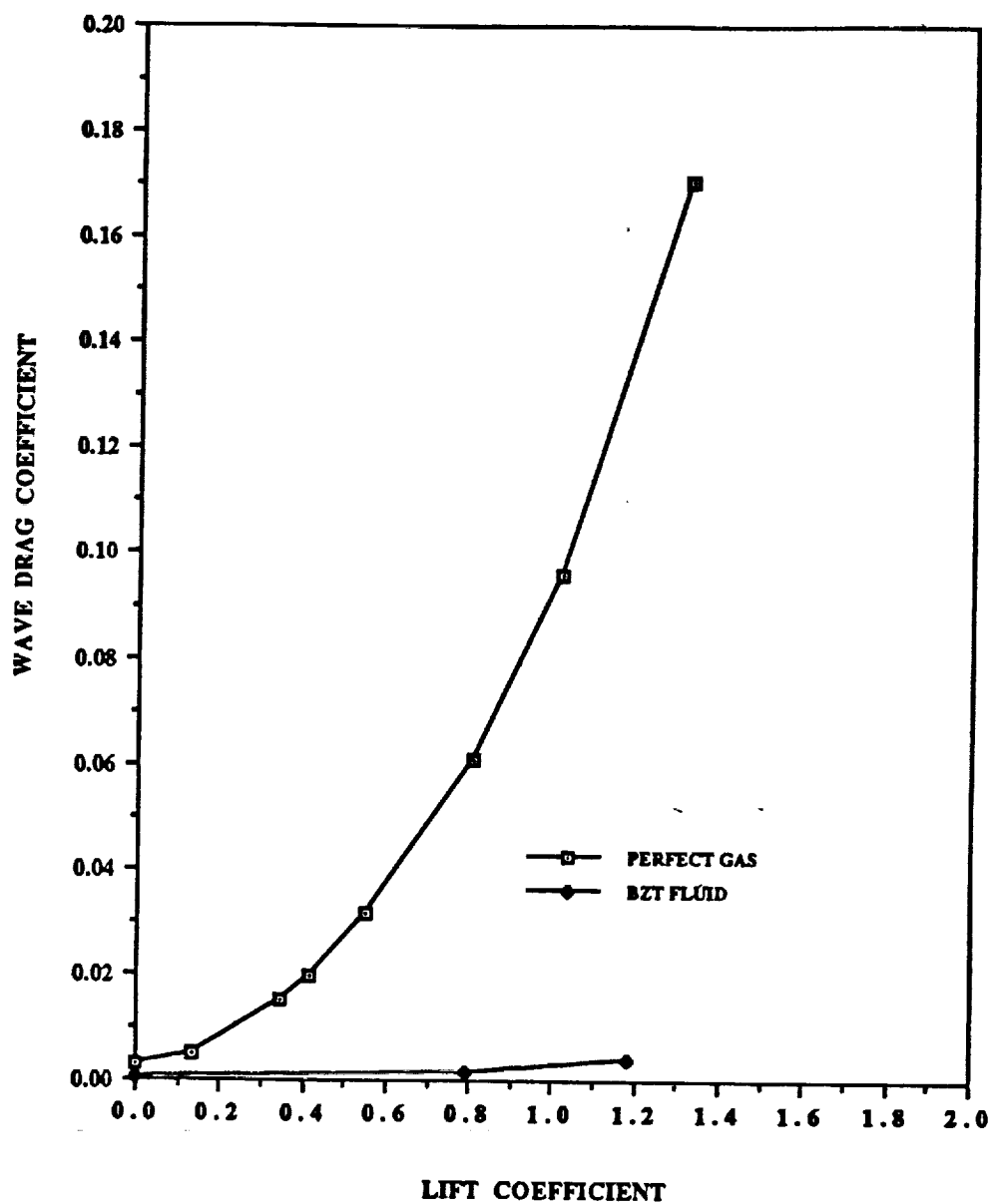
Figure 4.5c. BZT fluid and perfect gas drag coefficient versus lift coefficient for a NACA 0012 airfoil at $M_\infty = 0.8$, angle of attack range of 0.0 to 6.0 degrees. Both fluids have specific heat values of $R/C_v = 0.02$.
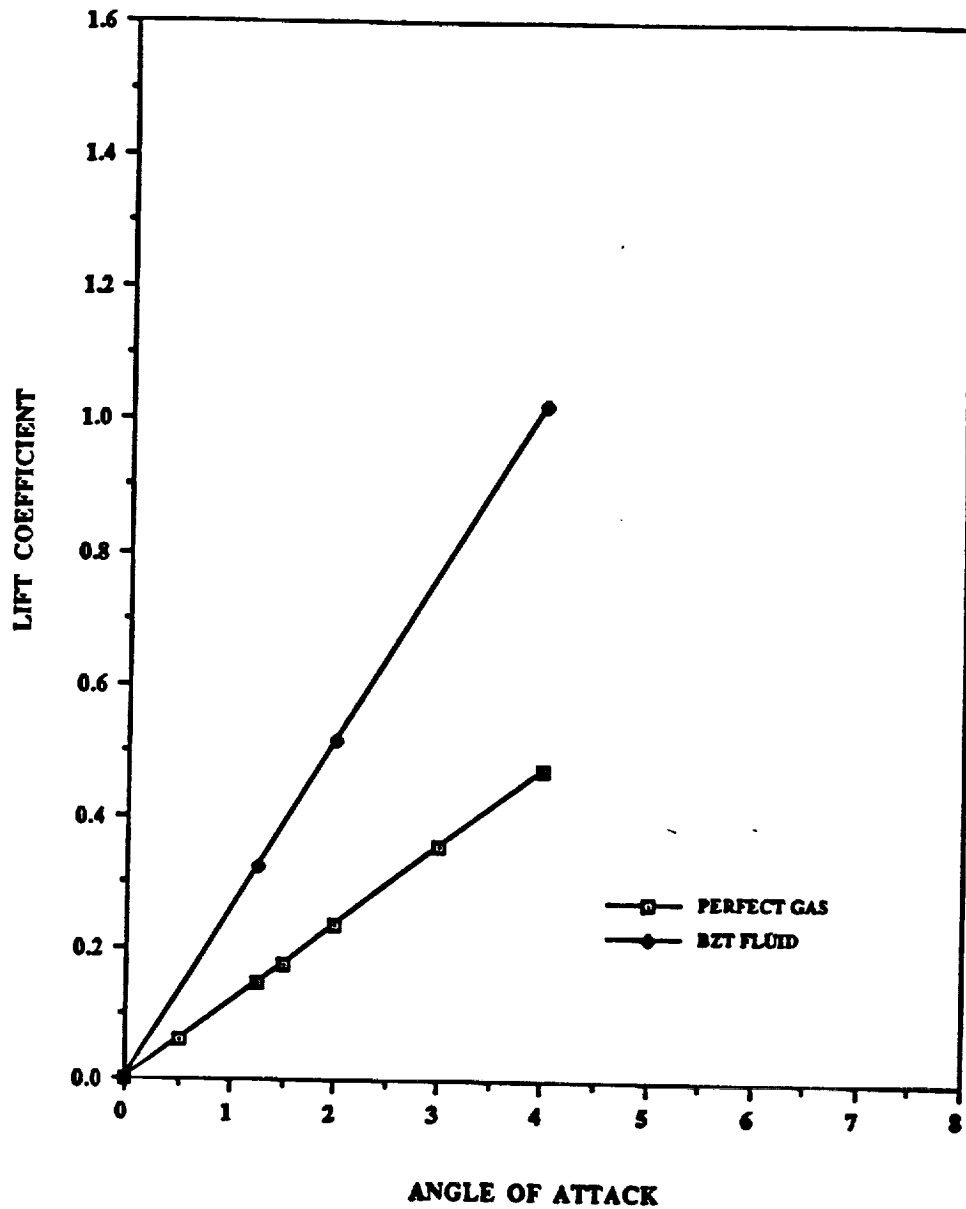
Figure 4.6a. BZT fluid and perfect gas lift coefficient versus angle of attack for A NACA 0012 airfoil at $M_\infty = 0.92$, and angle of attack range of 0.0 to 4.0 degrees. Both fluids have specific heat values of $R/C_v = 0.02$.
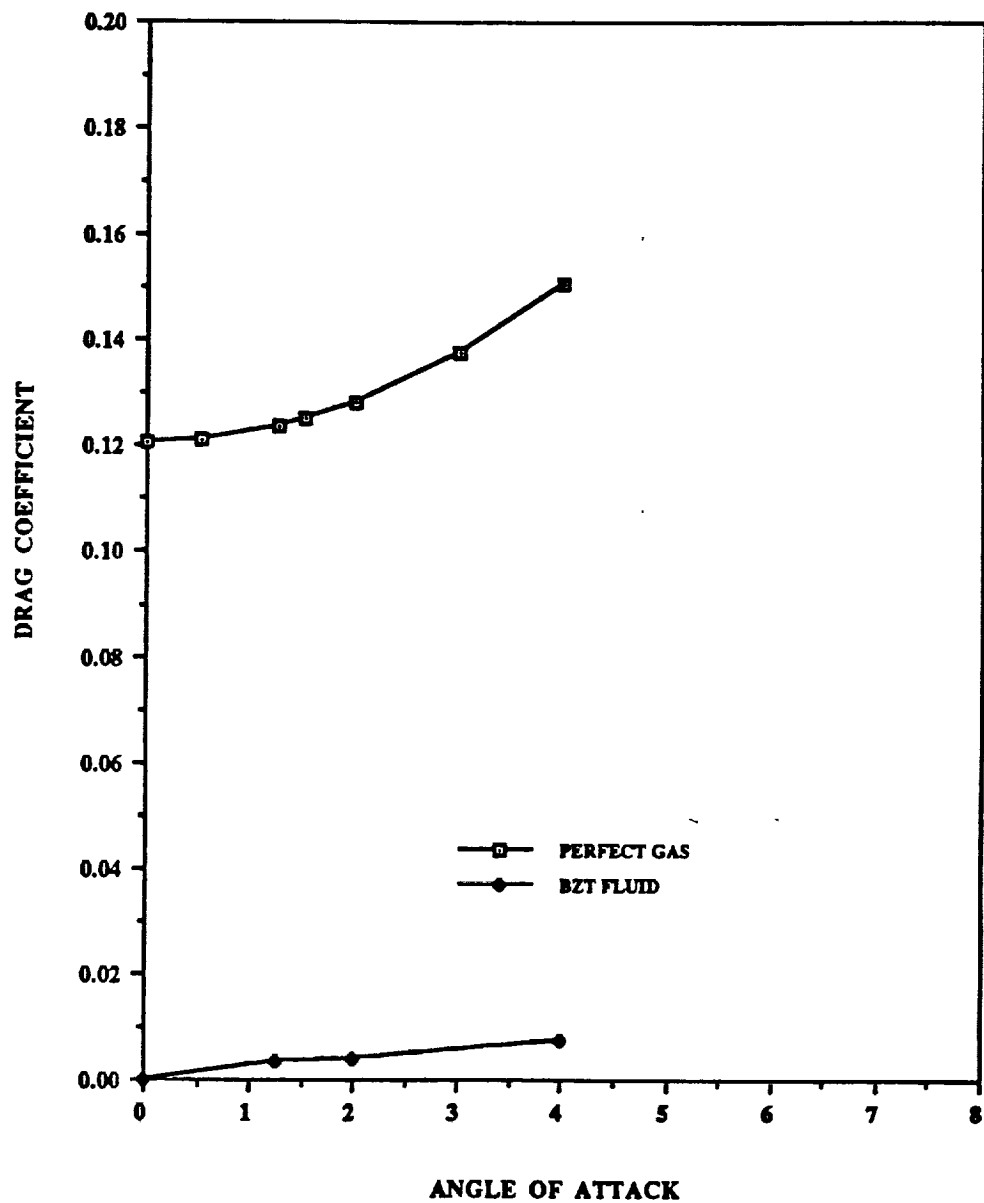
Figure 4.6b. BZT fluid and perfect gas drag coefficient versus angle of attack for A NACA 0012 airfoil at $M_\infty = 0.92$, and angle of attack range of 0.0 to 4.0 degrees. Both fluids have specific heat values of $R/C_v = 0.02$.

60

Figure 4.6c. BZT fluid and perfect gas drag coefficient versus lift coefficient for a NACA 0012 airfoil at $M_\infty = 0.92$, and angle of attack range of 0.0 to 4.0 degrees. Both fluids have specific heat values of $R/C_v = 0.02$.
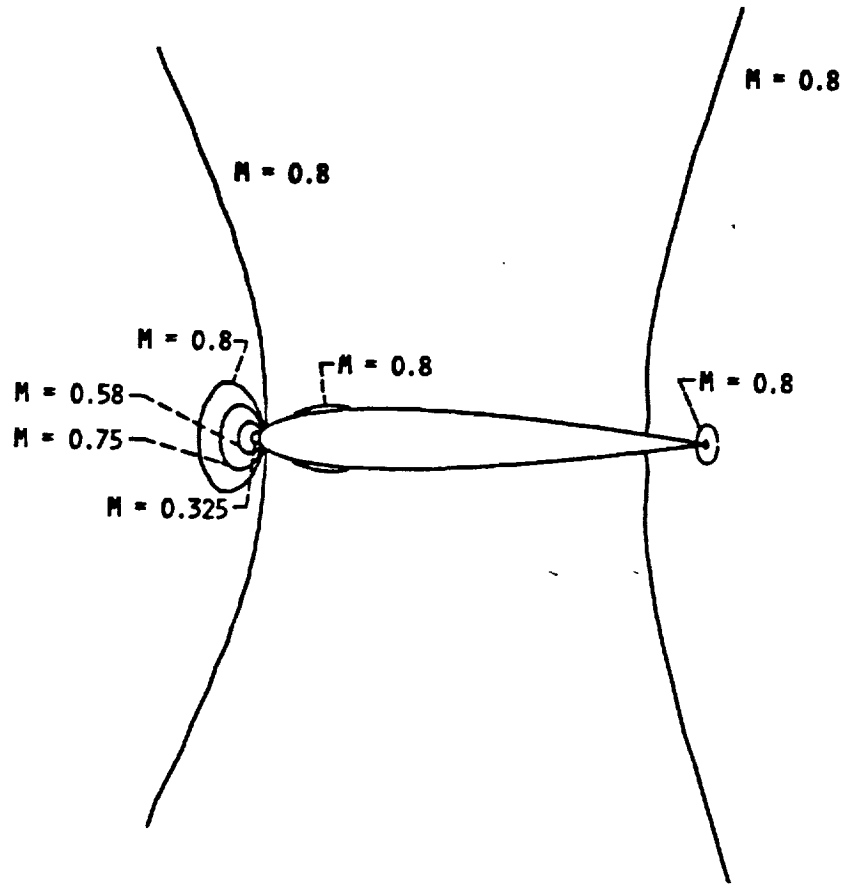
Figure 4.7a. BZT fluid Mach number contour plots for a NACA 0012 airfoil at $M_\infty = 0.8$, and angle of attack of 0.0 degree. The fluid is at conditions of $V_\infty = 1.25V_c$, $P_\infty = 1.0P_c$, and has a specific heat value of $R/C_v = 0.02$.
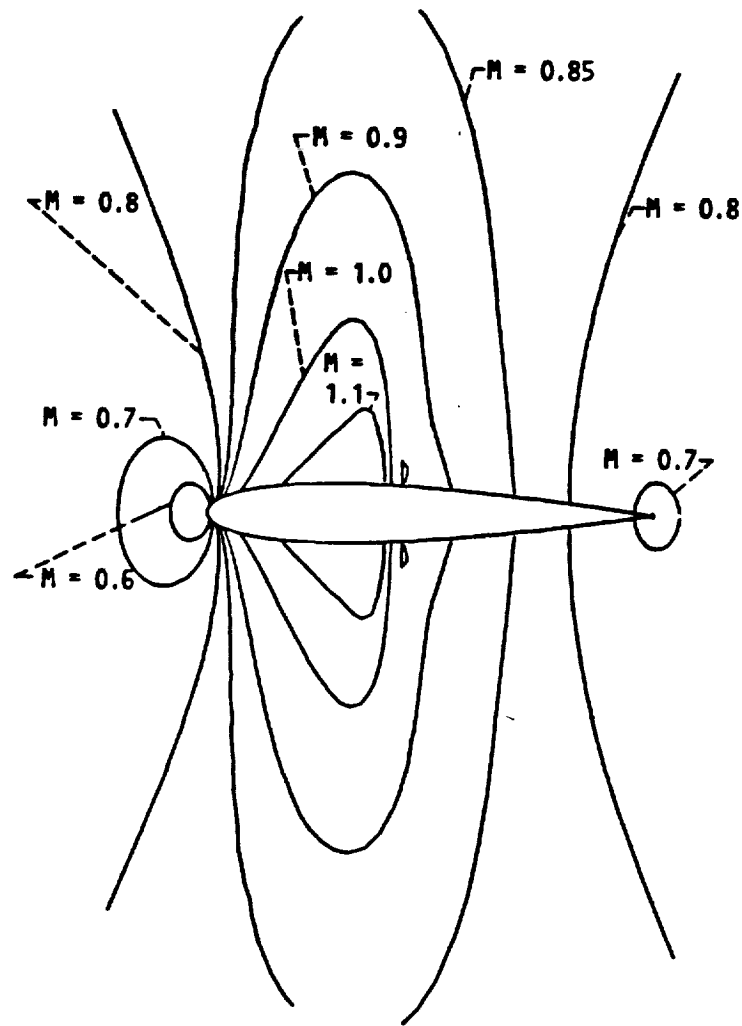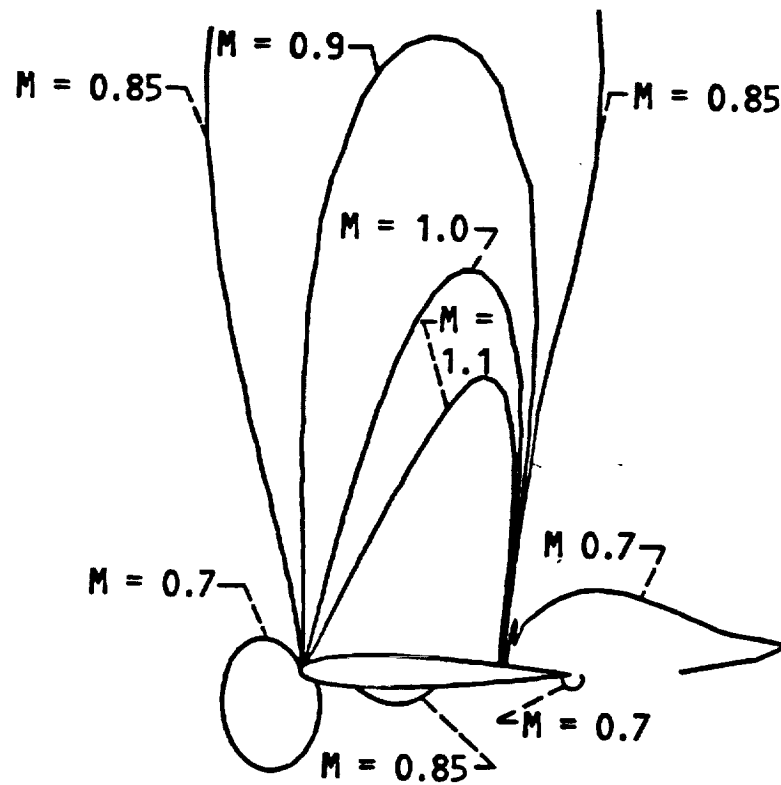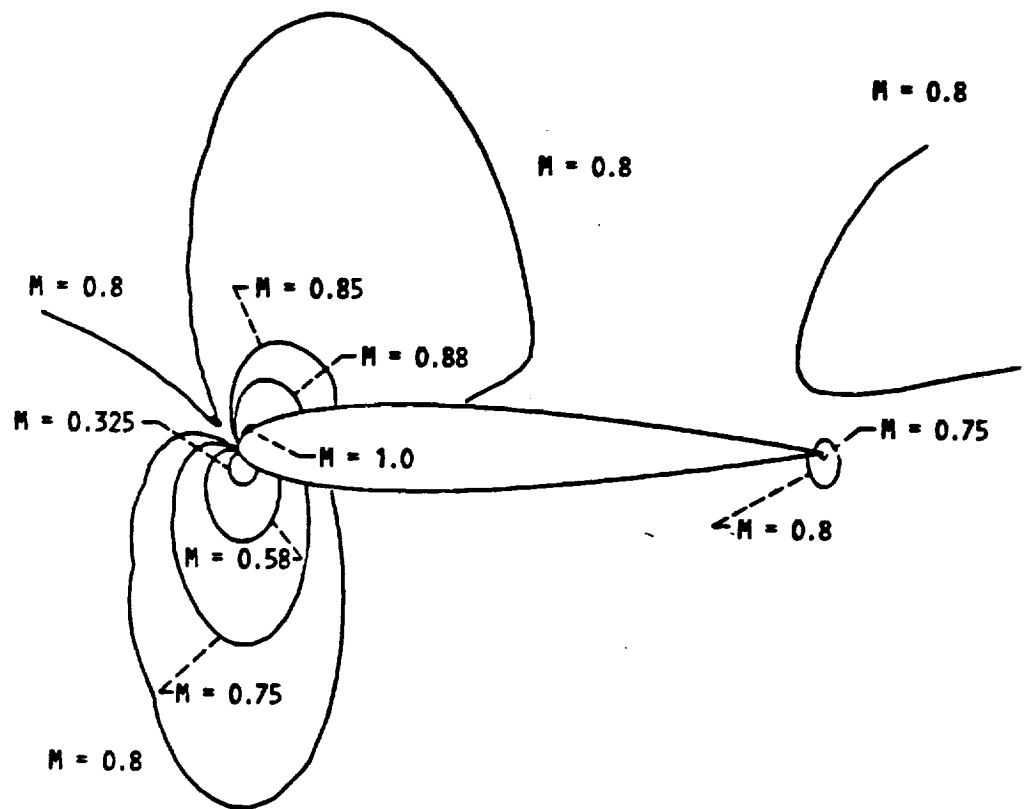
Figure 4.7b. Perfect gas Mach number contour plots for a NACA 0012 airfoil at $M_\infty = 0.8$, and an angle of attack of 0.0 degree. The fluid has a specific heat value of $R/C_v = 0.02$.
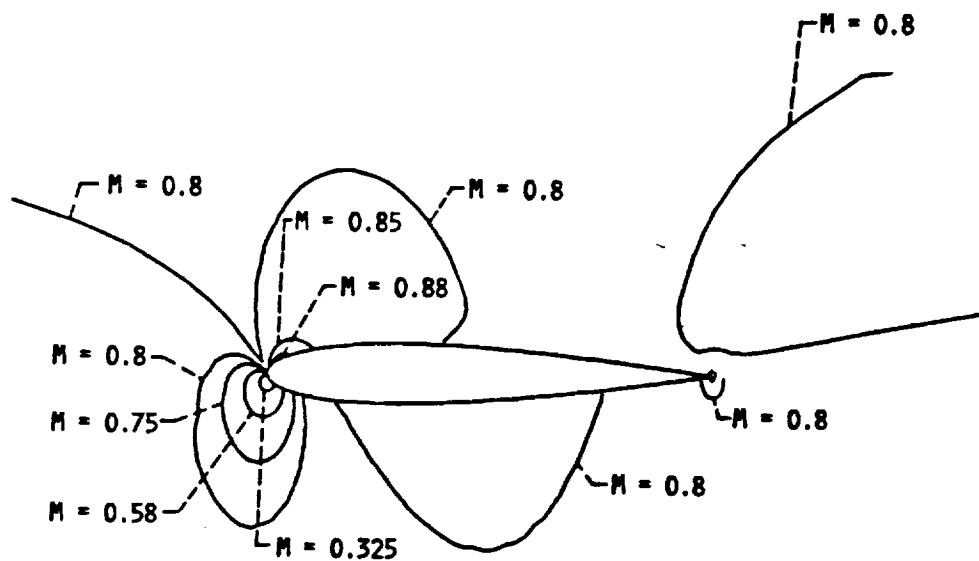
Figure 4.8a. BZT fluid Mach number contour plots for a NACA 0012 airfoil at $M_\infty = 0.8$, and an angle of attack of 4.0 degrees. The fluid is at conditions of $V_\infty = 1.25 V_c$, $P_\infty = 1.0 P_c$, and has a specific heat value of $R/C_v = 0.02$.
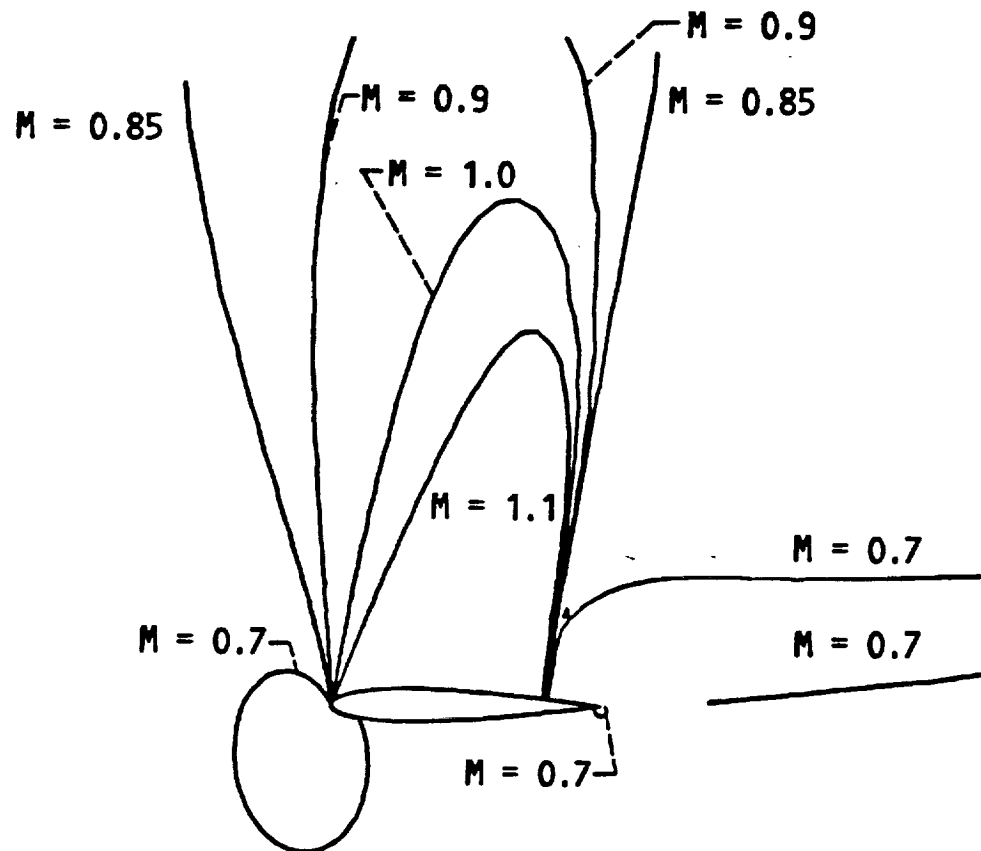
Figure 4.8b. Perfect gas Mach number contour plots for a NACA 0012 airfoil at $M_\infty = 0.8$, and an angle of attack of 4.0 degrees. The fluid has a specific heat value of and $R/C_v = 0.02$.

M = 0.8

M = 0.8

M = 0.8

M = 0.85

M = 0.88

M = 0.325
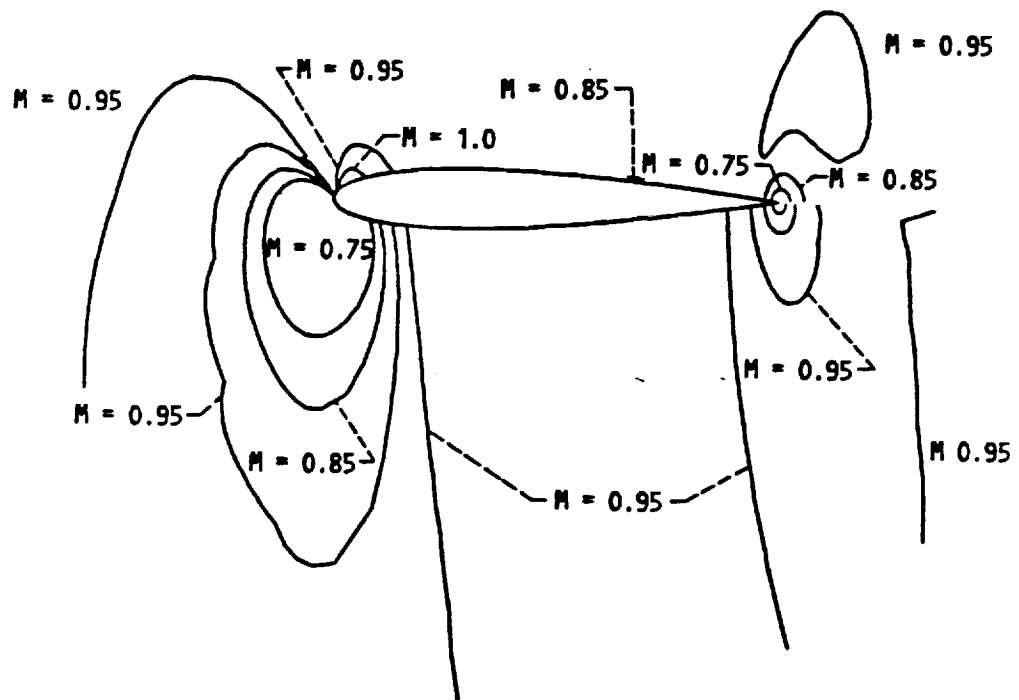
M = 1.0

M = 0.75

M = 0.8

M = 0.58

M = 0.75

M = 0.8

Figure 4.9a. BZT fluid Mach number contour plots for a NACA 0012 airfoil at $M_\infty = 0.8$, and an angle of attack of 6.0 degrees. The fluid is at conditions of $V_\infty = 1.25V_c$, $P_\infty = 1.0P_c$, and has a specific heat value of $R/C_v = 0.02$.
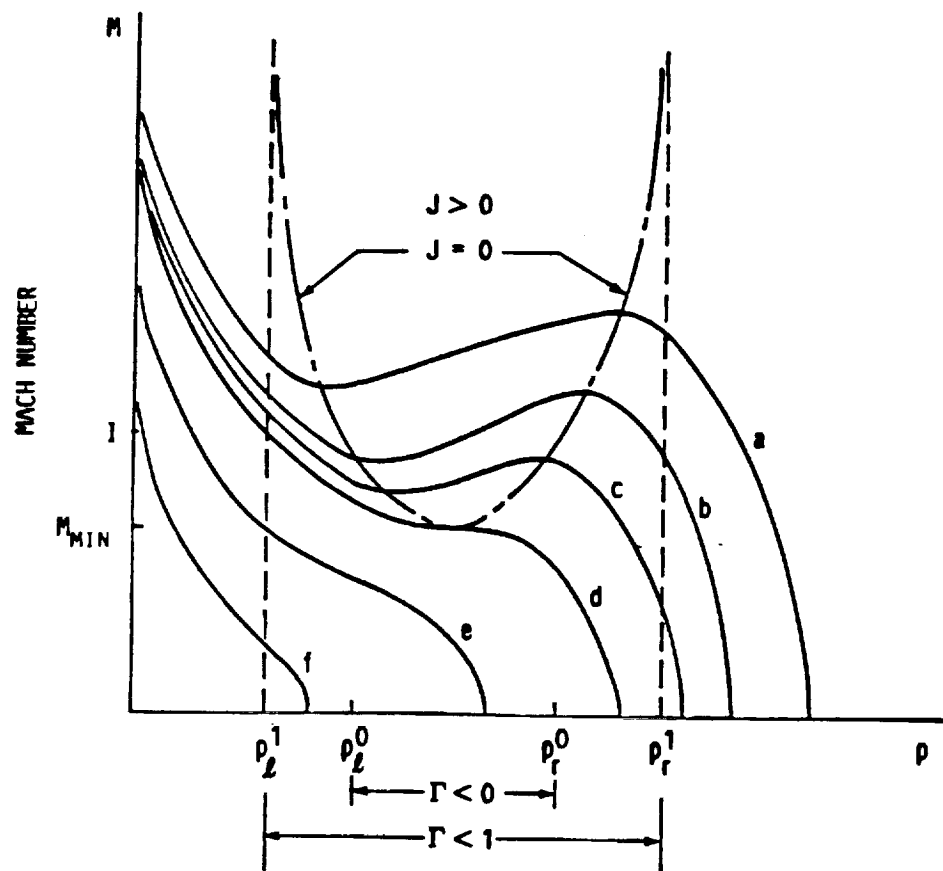
Figure 4.9b. Perfect gas Mach number contour plots for a NACA 0012 airfoil at $M_\infty = 0.8$, and an angle of attack of 6.0 degrees. The fluid has a specific heat value of $R/C_v = 0.02$.

Figure 4.10. BZT fluid Mach number contour plots for a NACA 0012 airfoil at $M_\infty = 0.92$, and an angle of attack of 4.0 degrees. The fluid is as conditions of $V_\infty = 1.25V_c$, $P_\infty = 1.0P_c$, and has a specific heat value of $R/C_v = 0.02$.

Figure 4.11. Mach number versus density curves for various stagnation conditions as given by the Bernoulli equation (Reference 21).
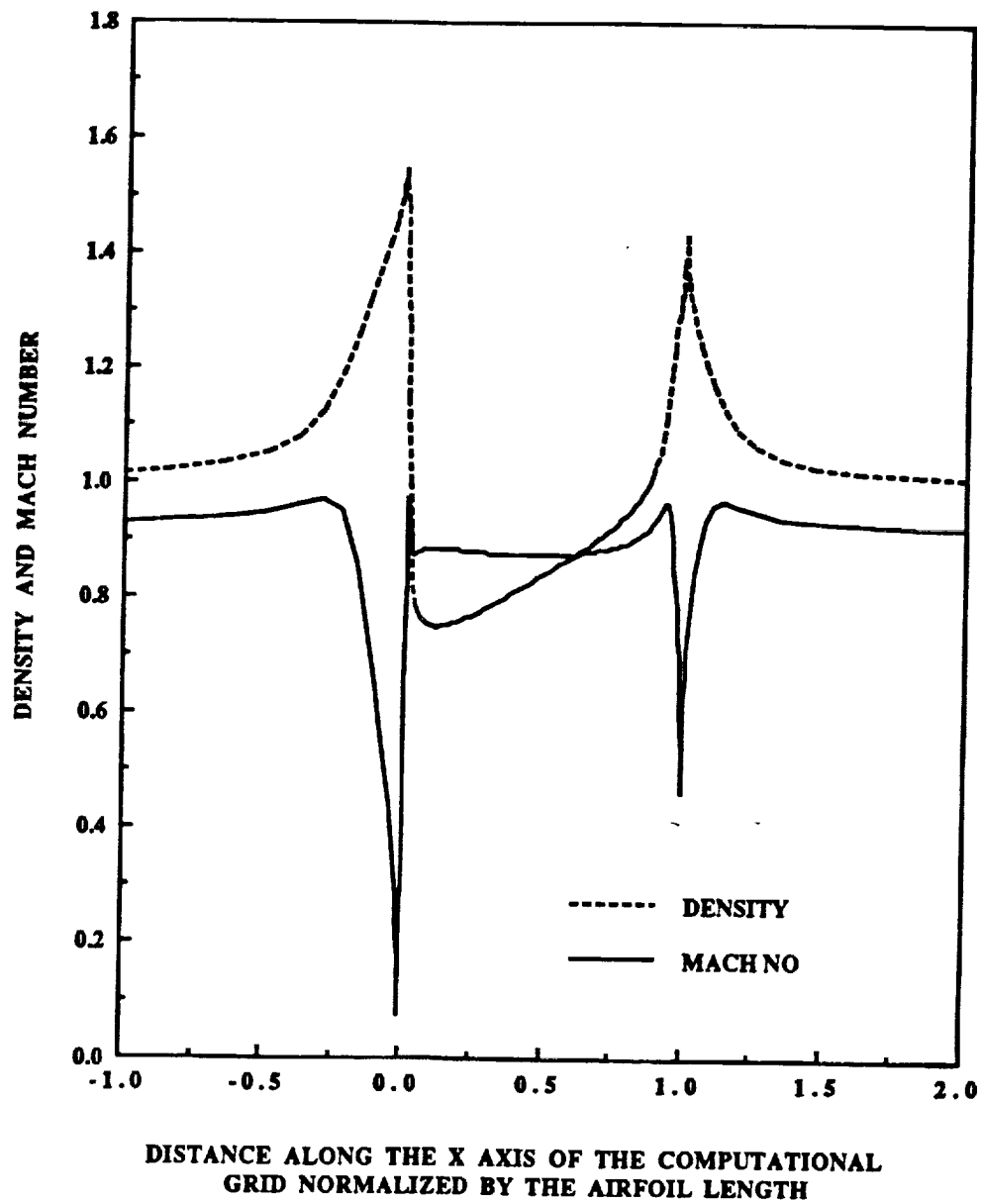
Figure 4.12. Density and Mach number versus the X Cartesian coordinates of the computational grid for a BZT fluid. The flow environment is at $M_\infty = 0.92$ for a NACA 0012 airfoil, and an angle of attack of 0.0 degrees. The fluid has a specific heat value of $R/C_v = 0.02$.
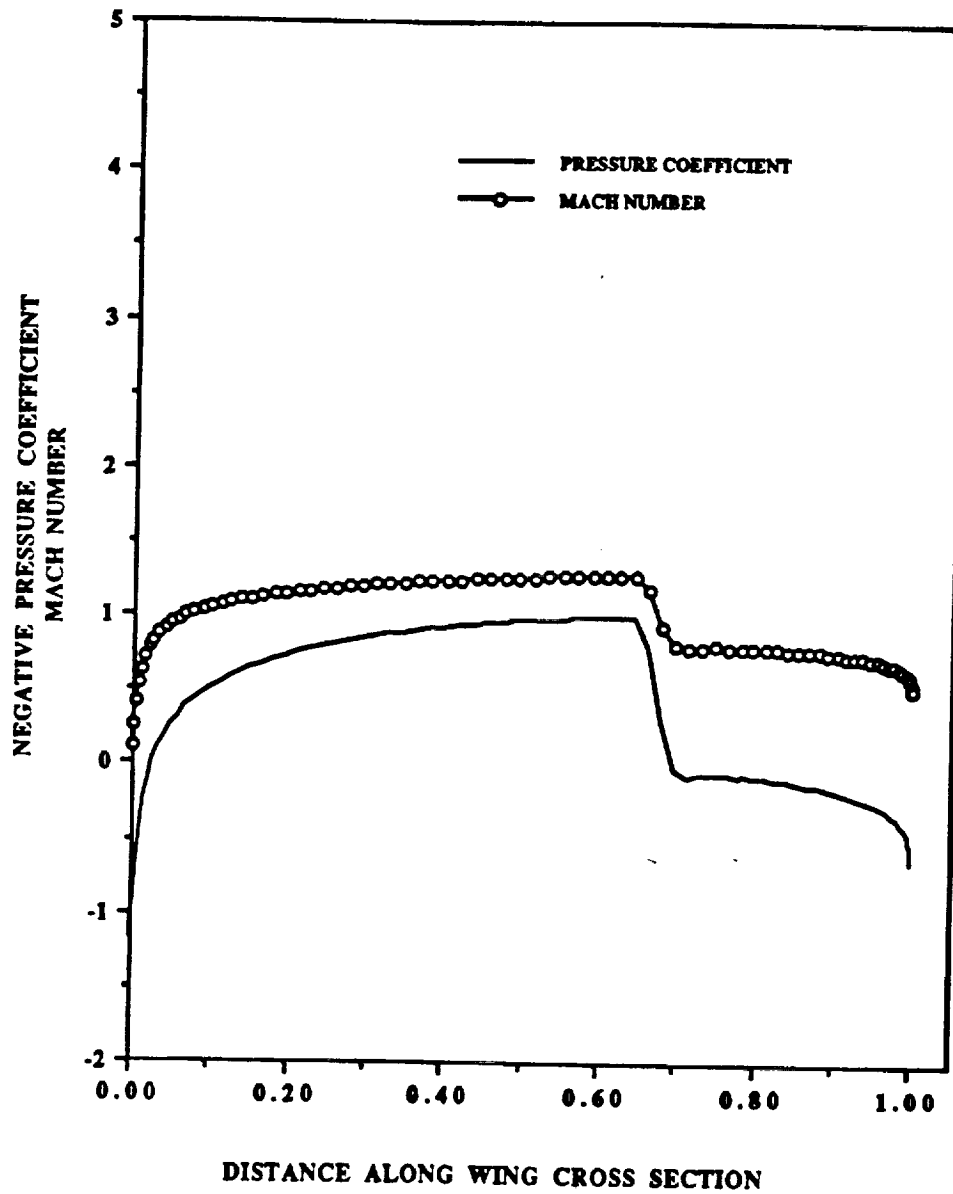
Figure 4.13. Perfect gas surface plots of negative pressure coefficient and local Mach number for a NACA 0012 airfoil at $M_\infty = 0.85$, and an angle of attack of 0.0 degree. The fluid has a specific heat value of $R/C_v = 0.02$.
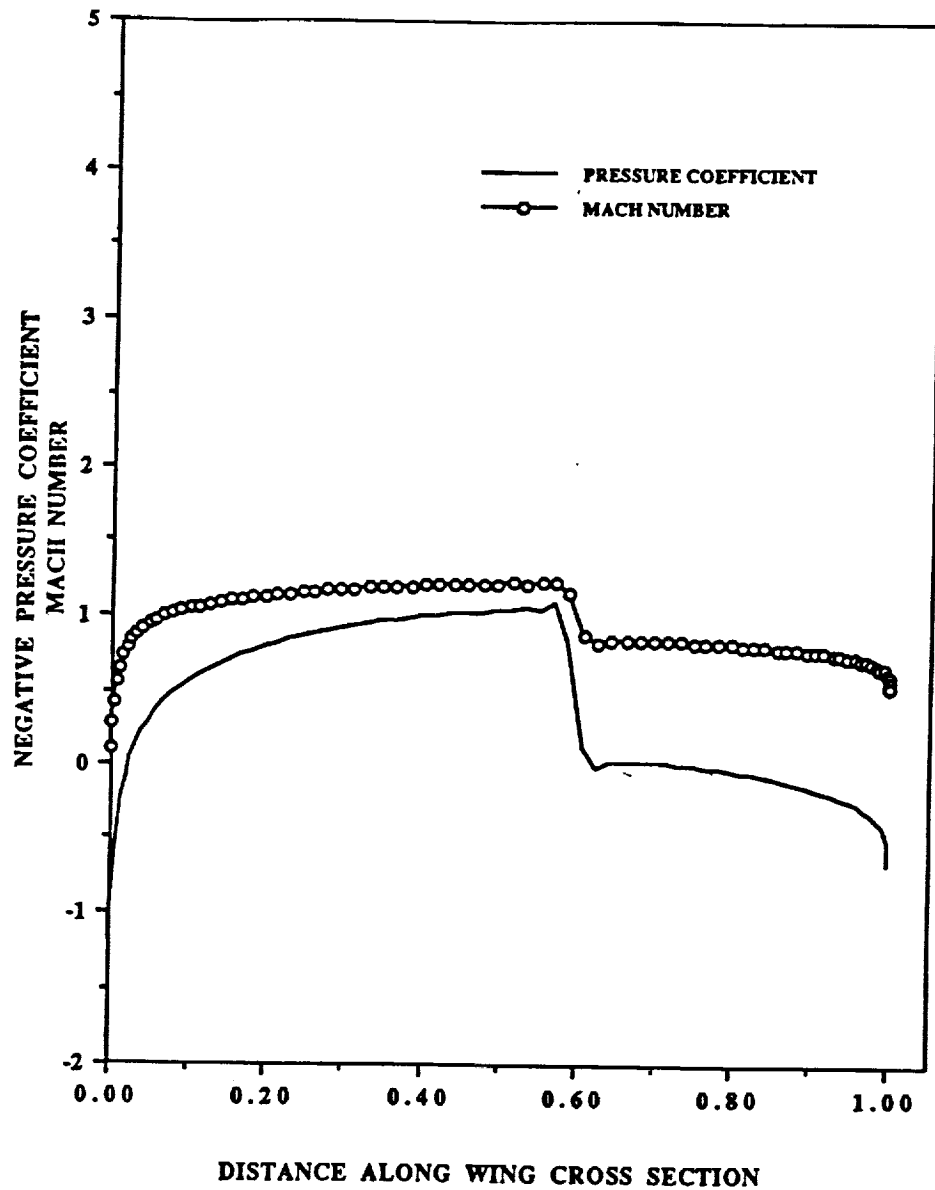
Figure 4.14. Dense gas surface plots of negative pressure coefficient and local Mach number for a NACA 0012 airfoil at $M_\infty = 0.85$, and angle of attack of 0.0 degree as given by the van der Waals equation of state. The fluid is at conditions of $V_\infty = 3.03V_c$, $P_\infty = 1.0P_c$, and has a specific value of $R/C_v = 0.02$.
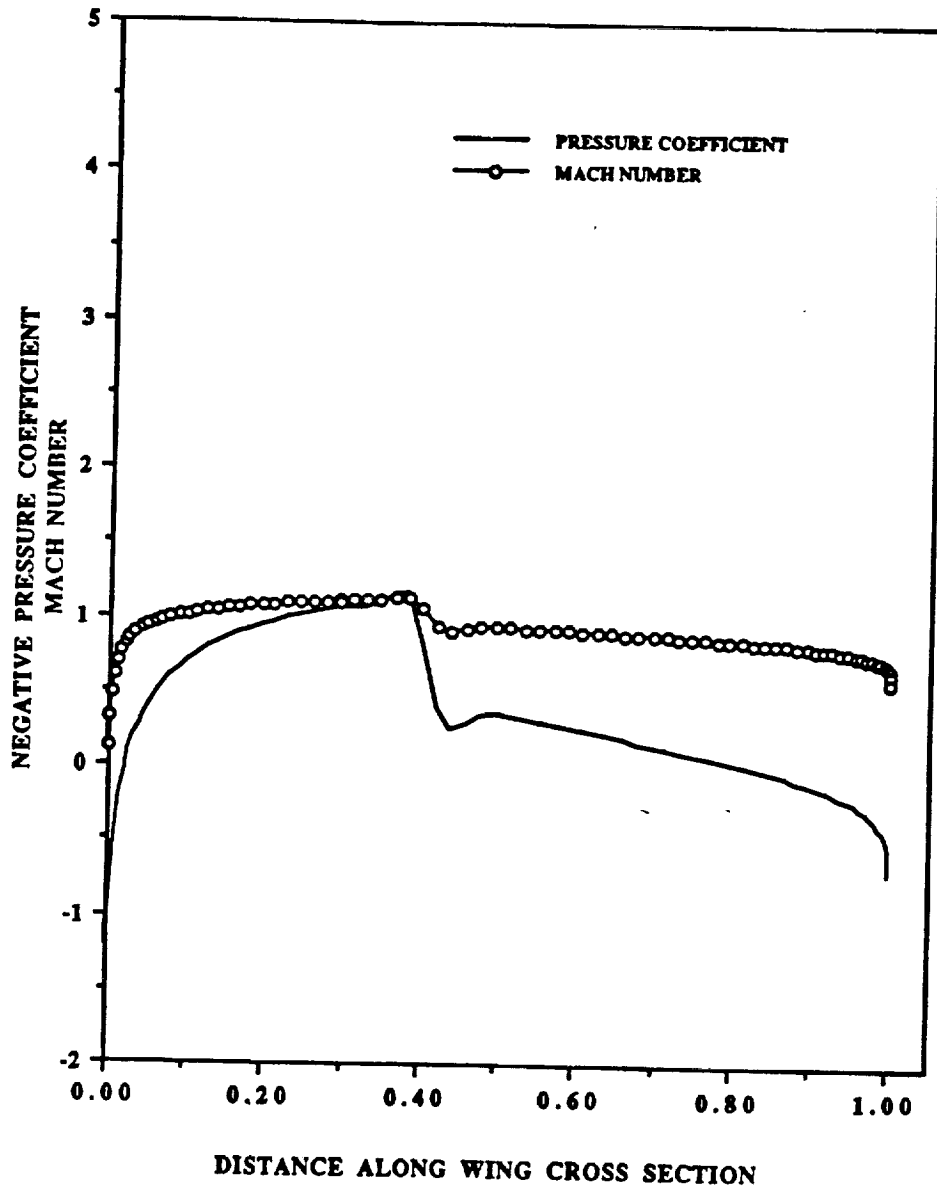
72

Figure 4.15. Dense gas surface plots of negative pressure coefficient and local Mach number for a NACA 0012 airfoil at $M_\infty = 0.85$, and angle of attack of 0.0 degree as given by the van der Waals equation of state. The fluid is at conditions of $V_\infty = 2.0V_c$, $P_\infty = 1.0P_c$, and has a value of $R/C_v = 0.02$.
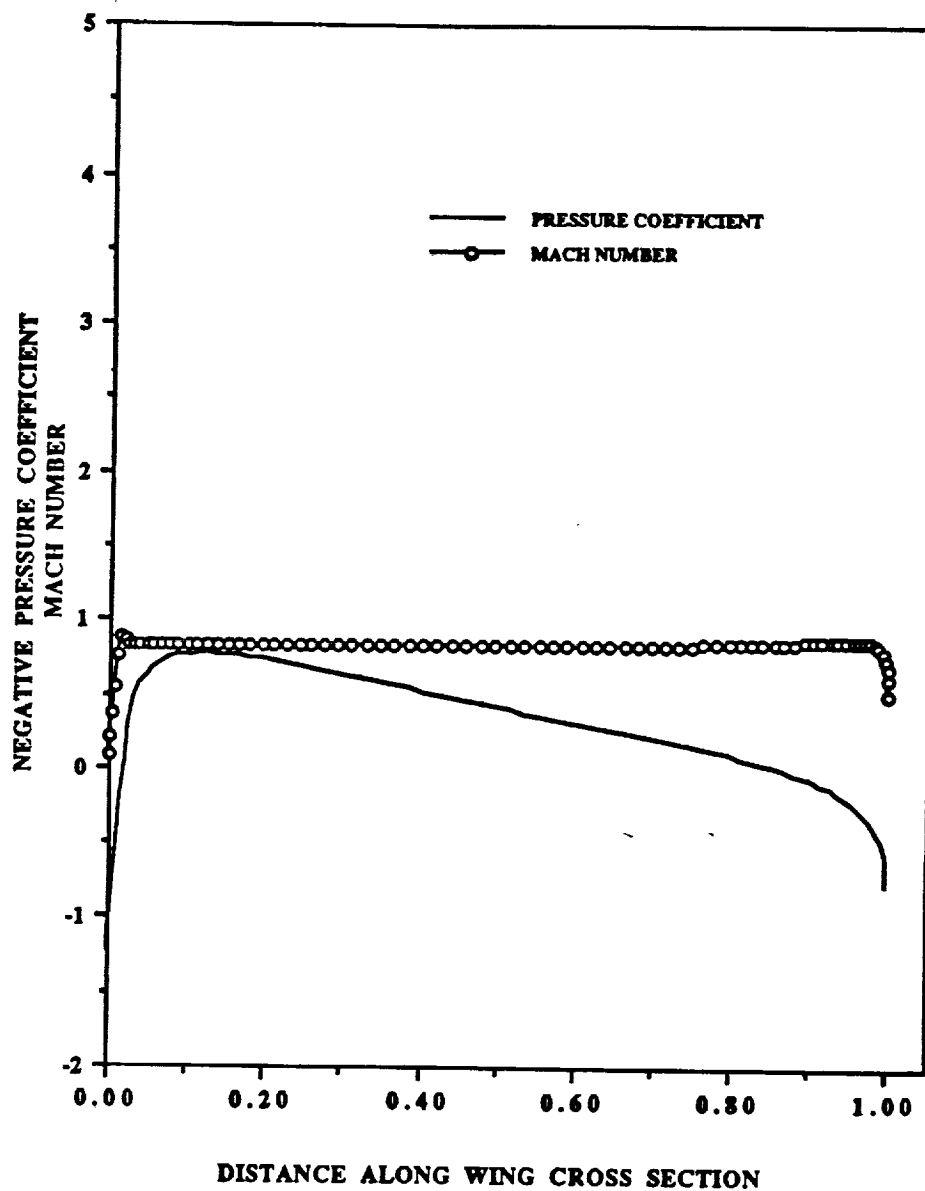
Figure 4.16. Dense gas surface plots of negative pressure coefficient and local Mach number for a NACA 0012 airfoil at $M_\infty = 0.85$, and angle of attack of 0.0 degree as given by the van der Waals equation of state. The fluid is at conditions of $V_\infty = 1.25 V_c$, $P_\infty = 1.0 P_c$, and has a specific heat value of $R/C_v = 0.02$.
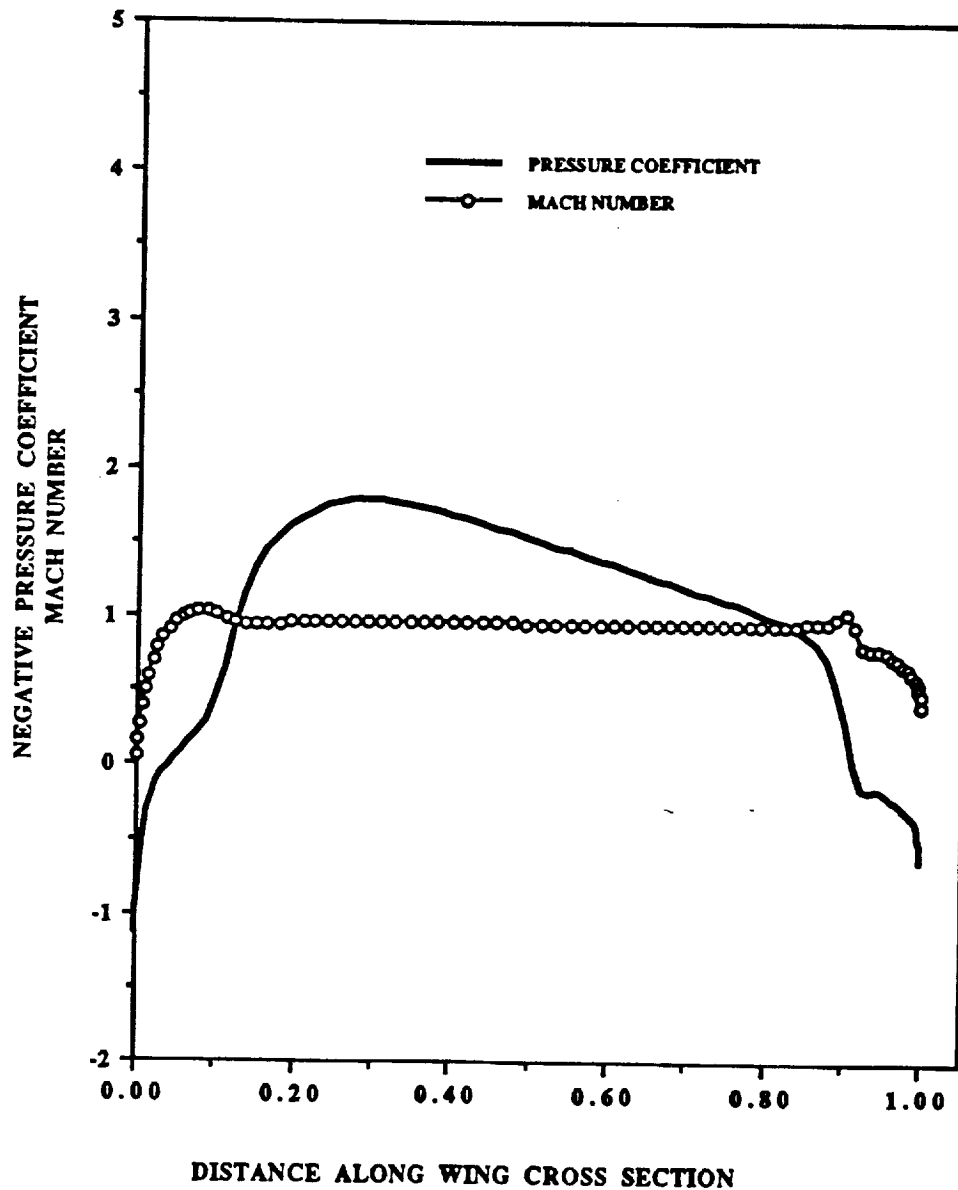
Figure 4.17. BZT fluid surface plots of negative pressure and local Mach number for a NACA 0012 airfoil at $M_\infty = 0.95$, angle of attack of 0.0 degree. The fluid is at conditions of $V_\infty = 1.0V_c$, $P_\infty = 1.08P_c$, and and has a specific heat value of $R/C_v = 0.02$.
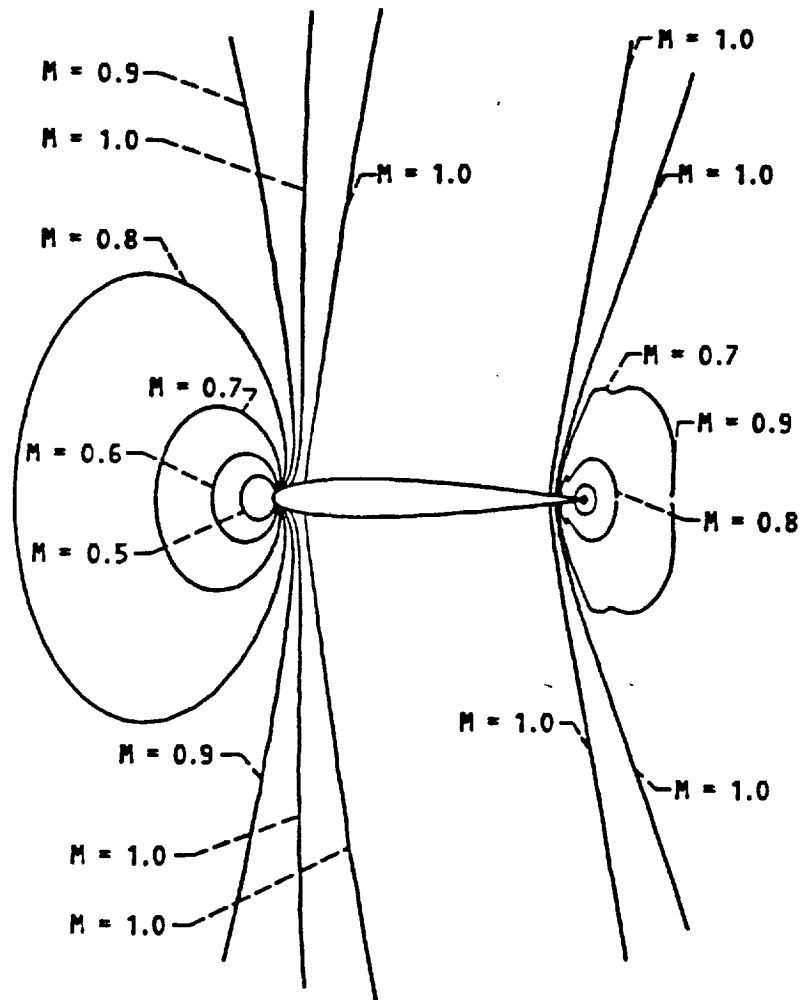
Figure 4.18. BZT fluid Mach number contour plots for a NACA 0012 airfoil at $M_\infty = 0.95$, angle of attack of 0.0 degree. The fluid is at conditions of $V_\infty = 1.0V_c$, $P_\infty = 1.08P_c$, and has a specific heat value of $R/C_v = 0.02$.

Appendix A

The derivation and application of Equations (4.0), to (4.5) are discussed below. Equations (4.0) through (4.5) were used to make critical Mach number estimates, calculate stagnation pressure, and calculate local pressure and Mach numbers for a given freestream Mach number condition.

We will begin with the derivation of Equation (4.4) which is obtained from the Bernoulli equation

$$h + \frac{V^2}{2} = h_\infty + \frac{V_\infty^2}{2} \qquad (A1.0a)$$

which may also be written as

$$h + \frac{a^2 M^2}{2} = h_\infty + \frac{a_\infty^2 M_\infty^2}{2} \cdot \qquad (A1.0b)$$

The enthalpy term h maybe written as

$$h = e + \frac{p}{\rho} \qquad (A1.0c)$$

where e is given by Equation (3.6) and $\frac{p}{\rho}$ is from the van der Waals equation of state (2.7). Thus, the enthalpy becomes

$$h = e_r - C_v T_r + \alpha \rho_r + C_v T \left(1 + \frac{R/C_v}{1 - b\rho} \right) - 2\alpha\rho \qquad (A2.0)$$

Substituting the speed of sound from Equation (3.25), and Equation (A2.0) into Equation (A1.0b) and then solving for the freestream Mach number results in

$$M_\infty^2 = \frac{2RT_\infty}{\delta a_\infty^2} \left\{ \left(\frac{T}{T_\infty} \right) \left\{ 1 + \frac{\delta}{1-b\rho} \right\} - \left(1 + \frac{\delta}{1-b\rho} \right) \right\}$$
$$- \frac{4\alpha}{a_\infty^2} \left\{ \frac{\rho}{\rho_\infty} - 1 \right\} + \frac{a^2}{a_\infty^2} M^2 \qquad \text{(A3.0)}$$

The non-dimensional form of (A3.0) is given by Equation (4.4).

The pressure expression of (4.2) was obtained by substituting the appropriate expressions of (3.2a) into Equation (2.7). The form of Equation (2.7) employed was

$$\frac{P}{\rho} = \frac{RT}{1-b\rho} - \alpha\rho \qquad \text{(A4.0a)}$$

Replacing the parameters P, ρ, T, b, and α with equivalent expressions from Equations (3.2a) gave

$$\frac{\bar{P}P_\infty}{\bar{\rho}\rho_\infty} = \frac{RT}{1 - \frac{\bar{b}}{\rho_\infty}\bar{\rho}\rho_\infty} - \frac{P_\infty}{\rho_\infty^2} \bar{\alpha}\bar{\rho}\rho_\infty \qquad \text{(A4.0b)}$$

Multiplying Equation (A4.0b) by $\frac{\rho_\infty}{P_\infty}$ and symplifying the expression resulted in

$$\frac{\bar{P}}{\bar{\rho}} = \frac{\rho_\infty RT_\infty}{P_\infty} \left(\frac{T}{T_\infty} \right) \left(\frac{1}{1-\bar{b}\bar{\rho}} \right) - \bar{\alpha}\bar{\rho} \qquad \text{(A4.0c)}$$

78

Let $Z_\infty = \dfrac{\rho_\infty R T_\infty}{P_\infty}$ and solving for $\bar{P}$ gave Equation (4.2).

The isentropic condition given by Equation (4.3) was found by applying the isentropic assumption to Equation (3.15) which resulted in

$$\bar{S} = exp\left(\frac{s - s_r = 0}{C_v}\right) = exp\left[\ell n\left\{\left(\frac{T}{T_r}\right)\left(\frac{1-b\rho}{\rho} \cdot \frac{\rho_r}{1-b\rho_r}\right)^{\frac{R}{C_v}}\right\}\right] \quad (A5.0)$$

and reduced to Equation (4.3).

Report Documentation Page

1. Report No. NASA TM-103722	2. Government Accession No.	3. Recipient's Catalog No.
4. Title and Subtitle Transonic Aerodynamics of Dense Gases		5. Report Date January 1991
		6. Performing Organization Code
7. Author(s) Sybil Huang Morren		8. Performing Organization Report No. E-5953
		10. Work Unit No. 591-41-21
9. Performing Organization Name and Address National Aeronautics and Space Administration Lewis Research Center Cleveland, Ohio 44135-3191		11. Contract or Grant No.
		13. Type of Report and Period Covered Technical Memorandum
12. Sponsoring Agency Name and Address National Aeronautics and Space Administration Washington, D.C. 20546-0001		14. Sponsoring Agency Code

15. Supplementary Notes

This report was submitted as a thesis in partial fulfillment of the requirements for the degree of Master of Science in Engineering Science and Mechanics to Virginia Polytechnic Institute and State University, Blacksburg, Virginia in April 1990. Responsible person, Sybil H. Morren (216) 433-6603.

16. Abstract

Transonic flow of dense gases for two-dimensional, steady-state, flow over a NACA 0012 airfoil was predicted analytically. The computer code used to model the dense gas behavior was a modified version of Jameson's FLO52 airfoil code. The modifications to the code enabled modeling the dense gas behavior near the saturated vapor curve and critical pressure region where the fundamental derivative, Γ, is negative. This negative Γ region is of interest because the nonclassical gas behavior such as formation and propagation of expansion shocks, and the disintegration of inadmissible compression shocks may exist. The results of this study indicated that dense gases with undisturbed thermodynamic states in the negative Γ region show a significant reduction in the extent of the transonic regime as compared to that predicted by the perfect gas theory. The results of the thesis support existing theories and predictions of the nonclassical, dense gas behavior from previous investigations.

17. Key Words (Suggested by Author(s)) Two dimensional; Steady state; Flow; Dense gases; Nonclassical gas dynamics; Van der Waals gas equation		18. Distribution Statement Unclassified – Unlimited Subject Category 02	
19. Security Classif. (of this report) Unclassified	20. Security Classif. (of this page) Unclassified	21. No. of pages 82	22. Price* A05